

## Chapter 2

# Statistical Mechanics of Thin Films

The second chapter is an introduction into the main physical concepts of wetting and dewetting, in particular to the corresponding *wetting* and *dewetting phase transitions*. These phase transitions occur in a broad range of physical systems: classical liquids, polymers, quantum liquids such as helium... and even superconductors, in which the ‘liquid’ phases are provided by the electrons, both normal and superconducting. We will encounter some of these physical examples in Chap. 3.

In this and the following chapters a number of calculational exercises, called *Tasks*, are indicated. They are meant to induce the reader to practice and deepen the understanding of the developed concepts. Occasionally, these tasks will be more than simple completions of the derivations performed in the book.

### 2.1 Capillarity and Surface Tension

The basic equation governing capillary phenomena at surfaces is *Young’s equation* (also called the *Young-Dupré equation*) which relates the interfacial tensions between a solid  $s$ , liquid  $l$  and vapour phase  $v$  denoted by  $\sigma_{ij}$  with  $i, j = s, l, v$  via the *contact angle* which the liquid-vapour interface makes with the solid wall. The equation reads as

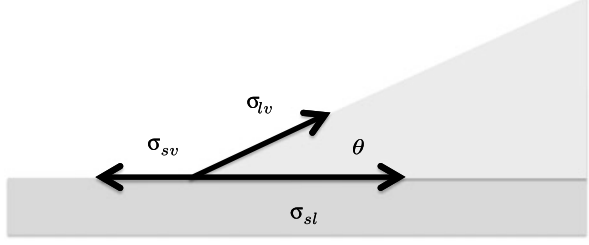
$$\cos \theta = \frac{\sigma_{sv} - \sigma_{sl}}{\sigma_{lv}} = 1 + \frac{S}{\sigma_{lv}} \quad (2.1)$$

where  $S \equiv \sigma_{sv} - (\sigma_{sl} + \sigma_{lv})$  is called the *spreading coefficient*.

*Task: Show that in thermal equilibrium,  $S < 0$  while  $S > 0$  is possible in a metastable or unstable state. This terminology refers to the fact that if  $S = 0$ , a droplet has fully spread to cover the available surface: its equilibrium contact angle has gone to zero, the surface is hence wet.*

Young’s equation follows from a simple argument which is illustrated in Fig. 2.1. Interfacial tensions are, by physical dimension, free energies per unit area, hence forces, and therefore Young’s equation follows from a *force balance* or a *condition*

**Fig. 2.1** Mechanical equilibrium condition leading to Young's equation: surface free energies  $\sigma_{ij}$  with  $ij = (sl, lv, sv)$  at the three-phase contact line of a liquid drop placed on a solid substrate. Drop and substrate are shown in different gray shades



of *mechanical equilibrium* at the points where the three phases meet, the *three-phase contact line*. This situation applies to both a capillary filled with liquid (such as encountered in the Introduction), or to a droplet placed on a flat wall, as sketched in Fig. 2.1 (actually, only a cut through the foot of the drop is shown).

Let us consider the droplet case in some detail. We ascribe to the liquid-vapour interface with surface tension  $\sigma_{lv}$  at a height  $h(x)$  the *interface Hamiltonian*

$$\mathcal{H}[h] = \int d^2x \left[ \sigma_{lv} \left( \sqrt{1 + (\nabla h(x))^2} - 1 \right) - (\Delta\mu)h(x) \right] \quad (2.2)$$

where the first term under the integral corresponds to the surface free energy of the liquid-vapour interface measured relative to a flat interface and written in a *Monge representation* which assumes that there is no overhang in the interface, see Fig. 2.2. The second term describes the chemical potential difference between the two fluid phases (vapour/liquid). The parameter  $\Delta\mu$  can also be read as a Lagrange multiplier associated with a fixed droplet volume,  $\Omega \equiv \int d^2x h(x)$ .

We further assume that the lateral dimension of the drop will be large as compared to its height so that the gradients of  $h$  will be small; we can then linearize the surface term according to

$$\sqrt{1 + (\nabla h(x))^2} \approx 1 + (1/2)(\nabla h(x))^2. \quad (2.3)$$

Finally, we assume a cylindrical symmetry of the interface profile,  $h \equiv h(r)$ , with  $r$  as the radial coordinate. We can now calculate the first variation of  $\mathcal{H}$  and find the ODE

$$\sigma_{lv} \left( h''(r) + \frac{1}{r} h'(r) \right) - \Delta\mu = 0, \quad (2.4)$$

where the prime stands for the differentiation with respect to  $r$ . This equation is the (linearized) *Young-Laplace equation*.

In order to obtain a droplet profile from Eq. (2.4) we impose the two boundary conditions

$$h'(0) = 0, \quad h(R) = 0. \quad (2.5)$$

The solution one obtains for the droplet profile is given by the parabola

$$h(r) = H(1 - (r/R)^2) \quad (2.6)$$

where one has the two parameters, the droplet height  $H$  and its radius  $R$ , given by

$$H = 2|\mathcal{S}|(\Delta\mu)^{-1}, \quad R = 2\sqrt{2\sigma_{lv}|\mathcal{S}|}(\Delta\mu)^{-1}. \quad (2.7)$$

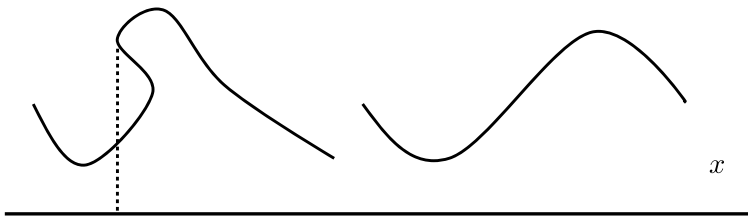


**Fig. 2.2** Sketch of two interface configurations, one with and one without an overhang. The overhanging configuration does not have a unique height function  $h(x)$ , as indicated by the dashed vertical line

*Task: Do this calculation explicitly.*

In our ‘parabolic’ approximation—having simplified the interface Hamiltonian by just keeping the harmonic term—the spreading coefficient  $S$  is given by

$$|S| = \frac{\sigma_{lv}\theta^2}{2} \quad (2.8)$$

which follows from an expansion of the cosine in Young’s equation. The ratio of height and width of the droplet is obtained from Eqs. (2.7)

$$\frac{H}{R} = \sqrt{\frac{|S|}{2\sigma_{lv}}} \quad (2.9)$$

and hence is a linear function of contact angle. One can also easily calculate the surface free energy of the sessile droplet which simply is

$$\mathcal{E} \equiv \mathcal{H}[h(r)] = \pi |S| R^2. \quad (2.10)$$

These results apply to droplets of sizes for which gravitational forces do not play a role. We have already seen in the Introduction that the relevant length here is the *capillary length*

$$\ell_c \equiv \sqrt{\frac{\sigma_{lv}}{\rho g}}, \quad (2.11)$$

such that in our case we must have  $H < \ell_c$  for the theory to be applicable (in addition to the condition on the contact angle, or on the gradients of  $h$ ).

*Task: Calculate the variation of the interface Hamiltonian without the linearization for small gradients, i.e. by using the full Hamiltonian, Eq. (2.2). Determine the full droplet profile and its surface free energy.*

Can we validate this result experimentally to convince ourselves that it is a valid description of the droplet properties? The challenge is, of course, to look at small droplets with dimensions well below the capillary length such that gravity plays no role.

In order to achieve this, polymer droplets of PS (polystyrene) have been studied with *Atomic Force Microscopy*, AFM (Seemann et al. 2001a). Contact angles  $\theta$

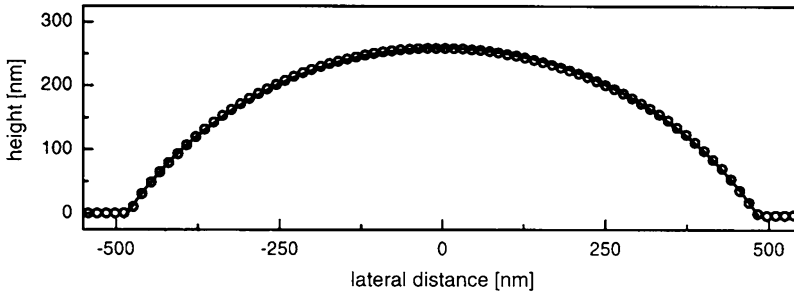


**Fig. 2.3** An AFM scan of a sessile droplet profile and its fit to a parabola. Reprinted with permission from Seemann et al. (2001a). Copyright by IOP

were determined for two different substrates: SiO-wafers and OTS-wafers. The experimental methods to produce such droplets (and, particularly, thin polymer films) are described in Appendix A. Two methods were used for analysis: (i) the determination of the slope at the three-phase contact line and (ii) a fit of a spherical cap to the data. The latter result is shown in Fig. 2.3.

Figure 2.4 shows the ratio of the scaling parameter  $H/R$  as a function of contact angle. Two clusters of data are shown, characterizing the two substrates. Droplets on SiO-wafers have a contact angle of  $6.9(5)^\circ$  with a height of about 20–40 nm. Droplets on OTS-wafers have a larger contact angle of  $58(1)^\circ$  and a central height of about 200–550 nm. The solid line in Fig. 2.4 corresponds to the parabolic droplet, the dashed line to a spherical droplet. These results convincingly show that the model description covers the shape of ‘small’ droplets very well, and that for larger contact angles indeed the full spherical shape needs to be taken into account. This reasoning applies to the ‘macroscopic’ shape of the drop.

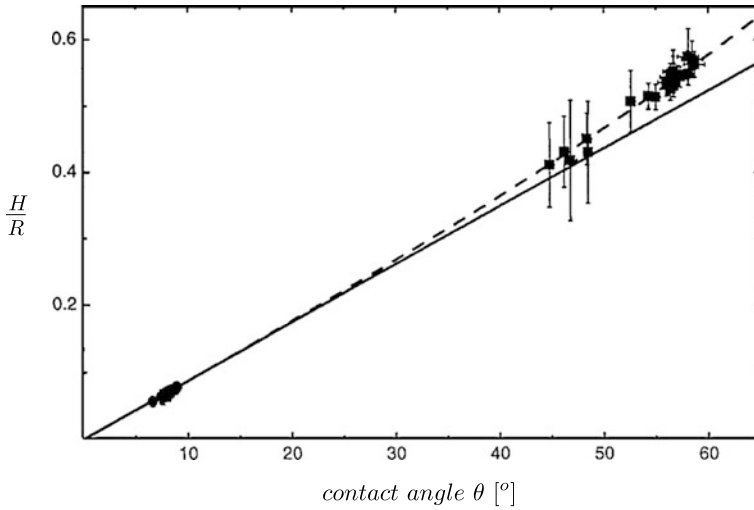
Things are different, however, when one looks into the details of the three-phase contact line. Indeed one might expect that additional forces, not covered by our interface Hamiltonian, may lead to modifications of the simple picture. The contact-line is placed in a region where more microscopic details of the interactions may matter, and the question therefore is how to capture these effects, beyond Young’s equation.

Figure 2.5 plots the cosine of the contact angle against the curvature of the interface. Underlying this plot is the assumption that the contact angle obeys a *modified Young equation* of the form

$$\cos \theta_r = \cos \theta - \frac{\tau \kappa}{\sigma_{lv}} \quad (2.12)$$

where  $\kappa$  is the *interfacial curvature*,<sup>1</sup> which in this case is simply  $1/R$ , and  $\tau$  a ‘line tension’ associated with the droplet contact line. This equation covers the deviation of the interfacial profile next to the wall, due to forces not included into the Hamiltonian of a capillary interface.

<sup>1</sup>See Chap. 4 for an explicit mathematical expression for the interfacial curvature.



**Fig. 2.4** The scaling of the droplet shape:  $H/R$  as a function of contact angle. Reprinted with permission from Seemann et al. (2001a). Copyright by IOP

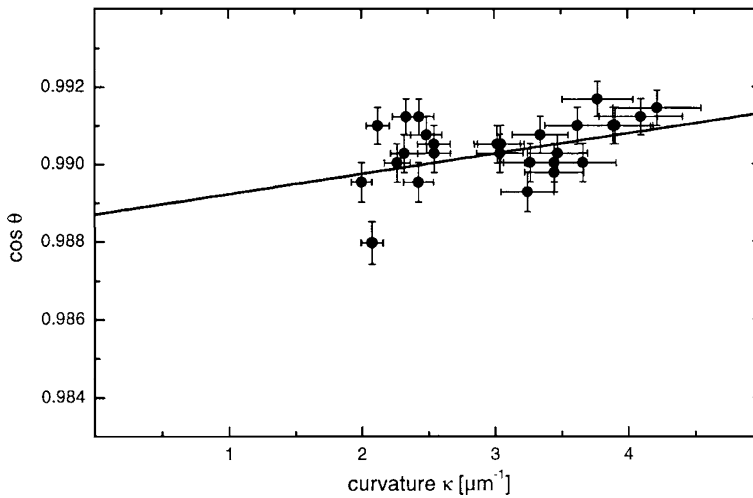


**Fig. 2.5** The line tension of a polystyrene droplet on an SiO-wafer, assuming the modified Young equation (*straight line*). Reprinted with permission from Seemann et al. (2001a). Copyright by IOP

From Fig. 2.5 we can infer a value of this ‘line tension’ of  $\tau = -10^{-11}$  J/m. Since a typical value of the surface tension is on the order of  $\sigma_{lv} = 10^{-2}$  J/m<sup>2</sup>, the ratio  $|\tau/\sigma_{lv}|$  gives a characteristic length scale on which the effect of the line tension matters, which is 1 nm. This result clearly shows the challenge inherent to such measurements.

**Fig. 2.6** SFM topography image of a water droplet on a silicon surface with a striped pattern with different wettability properties. The middle region is hydrophobic, causing the contact line to bend inwards. Reprinted with permission from Pompe and Herminghaus (2000). Copyright by the American Physical Society

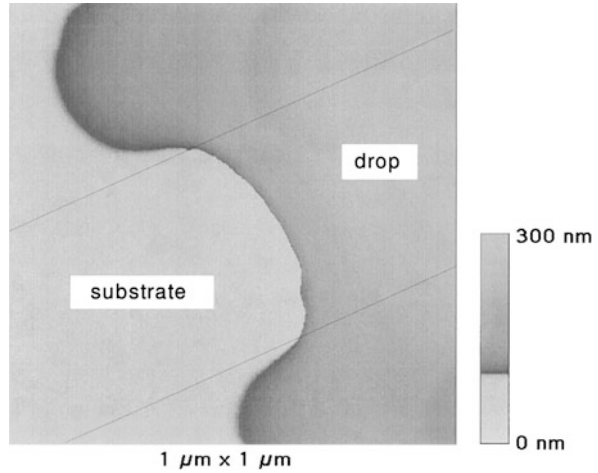
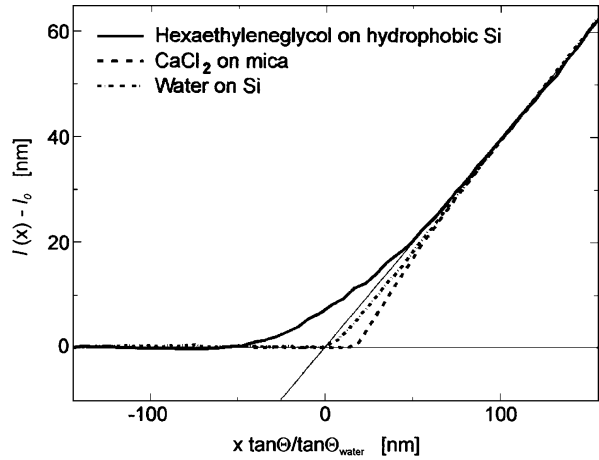


**Fig. 2.7** The vapour-liquid interface profile, here called  $\ell(x)$ , measured by SFM for three different systems. Reprinted with permission from Pompe and Herminghaus (2000). Copyright by the American Physical Society



More details of the profile of the contact line were described by Herminghaus et al. (1999) and Pompe and Herminghaus (2000) who created liquid surface topographies based on artificially striped wettability patterns which force the contact-line of the drop to bend strongly, see Fig. 2.6. Surface force measurements not only allow an analogous determination of  $\tau$  as before with values via the modified Young equation, and yielding line tension values of similar magnitude, but they can also resolve the details of the vapour-liquid interface. Figure 2.7 shows these profiles for three different surfaces. All data show deviations from the straight ('dividing') line which corresponds to the droplet shape obtained from the Young-Laplace equation. The observation therefore quantifies the surface force contributions not taken into account by the surface tension, and it is precisely these forces which control the behaviour of the line tension, and, as we will see, also of thin films.

In order to achieve an understanding of the line tension in a proper theoretical framework—e.g., of its sign—we must first look into more detail at the origin of the microscopic forces acting at interfaces. We will see that we have and how we have to correct the *interface Hamiltonian* by additional surface forces. Although we have understood from the previous discussion that there is a curvature-related correction to Young’s equation, and that the profile of the droplet foot deviates from a simple straight line, we do not yet have a clear understanding what the ‘line tension’ really is, and, actually, whether both measurements have access to the same quantity. Measurements alone do not suffice; conceptual, hence theoretical understanding is needed here.

## 2.2 Forces Acting at Interfaces

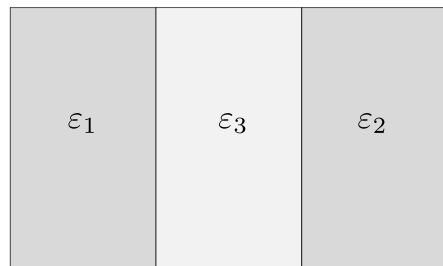
The *surface tensions* (or *surface forces*) take into account the macroscopic effects of intermolecular interactions which can well be assumed as being carried by short-range, structural interactions. However, on the molecular level interactions are not only structural, but also determined by charges, hence of an electrostatic nature. The fundamental theory of *dispersion forces* goes back to Dzyaloshinskii, Lifshitz and Pitaevski (short: DLP) (Dzyaloshinskii et al. 1961). The quantity of interest describing the attraction or repulsion of two interfaces as sketched in Fig. 2.8 is given by the thermodynamic expression of the *disjoining pressure*

$$\Pi_{vdW}(h) \equiv -\frac{1}{A} \left( \frac{\partial G_{film}}{\partial h} \right) = -\frac{1}{A} \left( \frac{\partial V}{\partial h} \right), \quad (2.13)$$

where  $A$  is surface area, and  $V(h)$  is the Gibbs free energy of the two-surface system which is also called the *effective interface potential*.  $V(h)$  is understood as the excess surface free energy per unit area it takes to bring two separated interfaces (hence located ‘at infinity’) together to a finite distance  $h$ .

DLP showed how  $\Pi_{vdW}$  can be determined based on the theory of *finite-temperature quantum electrodynamics*. They derived the fundamental expression for the *disjoining pressure*  $\Pi_{vdW}(h)$  for a planar, film-type geometry shown in Fig. 2.8.

**Fig. 2.8** Geometry for the calculation of the long-range force between dielectric media across a planar gap



The three media (solid, liquid film, vapour) are characterized by their frequency-dependent dielectric functions  $\varepsilon_i$  ( $i = 1, 2, 3$ ). The final result writes as<sup>2</sup>

$$\Pi_{vdW}(h) = -\frac{k_B T}{\pi c^3} \sum_{n=0}^{\infty} \varepsilon_3^{3/2} \zeta_n^2 \int_1^{\infty} dp p^2 [I_1(h, p\zeta_n) + I_2(h, p\zeta_n)] \quad (2.14)$$

where  $\zeta_n = 2\pi n k_B T / \hbar$  and the complex dispersion functions  $\varepsilon_j(i\zeta_n)$  are introduced which are related to the frequency-dependent dielectric functions via *Kramers-Kronig relations*. In this expression, one has

$$I_1(h, p\zeta_n) = \left( \Delta_1(p) \Delta_2(p) \exp\left(\frac{2p\zeta_n}{c} h \sqrt{\varepsilon_3} - 1\right) \right)^{-1} \quad (2.15)$$

and

$$I_2(h, p\zeta_n) = \left( \Delta_{13}(p) \Delta_{23}(p) \exp\left(\frac{2p\zeta_n}{c} h \sqrt{\varepsilon_3} - 1\right) \right)^{-1} \quad (2.16)$$

with

$$\Delta_j(p) = \frac{s_j - p}{s_j + p} \quad (2.17)$$

$$\Delta_{jk}(p) = \frac{s_j \varepsilon_k - p \varepsilon_j}{s_i \varepsilon_k + p \varepsilon_j} \quad (2.18)$$

with

$$s_j = (\varepsilon_j / \varepsilon_3 - 1 + p^2)^{1/2}. \quad (2.19)$$

The DLP-formula allows to distinguish two contributions:

$$\Pi_{vdW}(h) = \Pi_{n=0}(h) + \Pi_{n>0}(h), \quad (2.20)$$

i.e., the zero-frequency and higher-order contributions. To make the first term explicit, one can first replace the integration over the variable  $p$  by an integration over

$$x = \frac{2p\zeta_n h \varepsilon_3^{1/2}}{c} \quad (2.21)$$

to obtain

$$\Pi_{vdW}(h) = -\frac{k_B T}{8\pi \hbar^3} \sum_{n=0}^{\infty} \int_{x(\zeta_n)}^{\infty} dx x^2 \left[ \left( \frac{1}{\Delta_1 \Delta_2} e^x - 1 \right)^{-1} + \left( \frac{1}{\Delta_{13} \Delta_{23}} e^x - 1 \right)^{-1} \right] \quad (2.22)$$

with the lower limit of integration being given by

$$x(\zeta_n) = 2\zeta_n h \varepsilon_3^{1/2} / c \quad (2.23)$$

---

<sup>2</sup>With respect to the usual notational difficulty, note that film height  $h$  should not be confused with Planck's (reduced) constant  $\hbar$ .

and the functions  $\Delta_j$  and  $\Delta_{jk}$  rewrite as

$$\Delta_j = \frac{(4\zeta_n^2 h^2 (\varepsilon_j - \varepsilon_3) + (cx)^2)^{1/2} - cx}{(4\zeta_n^2 h^2 (\varepsilon_j - \varepsilon_3) + (cx)^2)^{1/2} + cx} \quad (2.24)$$

and

$$\Delta_{jk} = \frac{(4\zeta_n^2 h^2 (\varepsilon_j - \varepsilon_3) + (cx)^2)^{1/2} - cx \varepsilon_j / \varepsilon_k}{(4\zeta_n^2 h^2 (\varepsilon_j - \varepsilon_3) + (cx)^2)^{1/2} + cx \varepsilon_j / \varepsilon_k}. \quad (2.25)$$

For the first term of  $\Pi_{vdW}(h)$ , one has  $\Delta_1 = \Delta_2 = 0$  and the term simplifies to

$$\Pi_{n=0}(h) = -\frac{k_B T}{16\pi h^3} \int_0^\infty dx x^2 \left( \frac{(\varepsilon_3(0) + \varepsilon_1(0))(\varepsilon_3(0) + \varepsilon_2(0))}{(\varepsilon_3(0) - \varepsilon_1(0))(\varepsilon_3(0) - \varepsilon_2(0))} e^x - 1 \right)^{-1} \quad (2.26)$$

where  $\varepsilon_j(0)$  are the *static dielectric constants* of the three media  $j = 1, 2, 3$ . This can be finally approximated by neglecting the  $(-1)$  term in the bracketed expression since the integral is dominated by the first term. After completing the integral one concludes with

$$\Pi_{n=0}(h) = -\frac{k_B T}{8\pi h^3} \int_0^\infty dx x^2 \frac{(\varepsilon_3(0) + \varepsilon_1(0))(\varepsilon_3(0) + \varepsilon_2(0))}{(\varepsilon_3(0) - \varepsilon_1(0))(\varepsilon_3(0) - \varepsilon_2(0))}. \quad (2.27)$$

This first, static term of the disjoining pressure represents the contribution of the permanent dipolar orientations of the materials, usually named the *Keesom* and *Debye contributions*.

The second, dispersive term can be rewritten by noting that because of the exponential, only contributions for which  $\zeta_n \gg c/a$  contribute to the final result. We therefore replace the sum over frequencies by an integral over the frequency range  $d\zeta = (2\pi k_B T / \hbar) dn$  which works for  $\hbar k_B T / c\hbar \ll 1$ . Around room temperature this restriction means that film thicknesses should be smaller than  $10^4 \text{ \AA}$ , which is generally the case. One thus finds

$$\begin{aligned} \Pi_{vdW}(h) = & -\frac{k_B T}{16\pi h^3} \int_{\zeta_1}^\infty d\zeta \int_{x(\zeta_n)}^\infty dx x^2 \left[ \left( \frac{1}{\Delta_1 \Delta_2} e^x - 1 \right)^{-1} \right. \\ & \left. + \left( \frac{1}{\Delta_{13} \Delta_{23}} e^x - 1 \right)^{-1} \right]. \end{aligned} \quad (2.28)$$

To work further with this result one can distinguish again two thickness regimes. They derive from electrostatic retardation effects. Comparing wavelengths to film thicknesses, one finds that for lengths less than  $500 \text{ \AA}$ , retardation effects can be neglected. Going through the dominant contributions in the integrand for these length scales, one finds  $\Delta_1 \approx \Delta_2 \approx 0$  and obtains for the  $(n > 0)$ -part of the dispersion forces

$$\Pi_{n>0}(h) = -\frac{k_B T}{16\pi h^3} \int_{\zeta_1}^\infty d\zeta \int_0^\infty dx x^2 \left( \frac{(\varepsilon_3 + \varepsilon_1)(\varepsilon_3 + \varepsilon_2)}{(\varepsilon_3 - \varepsilon_1)(\varepsilon_3 - \varepsilon_2)} e^x - 1 \right)^{-1} \quad (2.29)$$

where  $\varepsilon_j = \varepsilon_j(i\zeta)$  for  $j = 1, 2, 3$ . Similarly as before we can further reduce the integral and perform the integration over  $x$  to end up with

$$\Pi_{n>0}(h) = -\frac{k_B T}{8\pi h^3} \int_{\zeta_1}^\infty d\zeta \frac{(\varepsilon_3(i\zeta) + \varepsilon_1(i\zeta))(\varepsilon_3(i\zeta) + \varepsilon_2(i\zeta))}{(\varepsilon_3(i\zeta) - \varepsilon_1(i\zeta))(\varepsilon_3(i\zeta) - \varepsilon_2(i\zeta))} \quad (2.30)$$

For the case of large film thicknesses one introduces a new variable  $y = 2pl\zeta/c$  to obtain the expression

$$\begin{aligned} \Pi_{n>0}(h) = & -\frac{\hbar}{32\pi^2 h^4} \int_0^\infty dy \int_1^\infty dp \frac{y^2}{p^2} \varepsilon_3^{3/2} \\ & \times \left[ \left( \frac{1}{\Delta_1(p)\Delta_2(p)} e^{x\sqrt{\varepsilon_3}} - 1 \right)^{-1} \right. \\ & \left. + \left( \frac{1}{\Delta_{13}(p)\Delta_{23}(p)} e^{x\sqrt{\varepsilon_3}} - 1 \right)^{-1} \right] \end{aligned} \quad (2.31)$$

This expression shows that the retarded contribution falls off as  $h^{-4}$ .

From this excursion we now finally retain that the dispersion forces can be described by a disjoining pressure

$$\Pi_{vdW}(h) = -\frac{A}{6\pi h^3} \quad (2.32)$$

with the *Hamaker constant*

$$A \equiv A_{n=0} + A_{n>0} \quad (2.33)$$

or

$$\begin{aligned} A \approx & \frac{3}{4} kT \left( \frac{\varepsilon_1 - \varepsilon_3}{\varepsilon_1 + \varepsilon_3} \right) \left( \frac{\varepsilon_2 - \varepsilon_3}{\varepsilon_2 + \varepsilon_3} \right) \\ & + \frac{3\hbar}{4\pi} \int_{\zeta_1}^\infty d\nu \left( \frac{\varepsilon_1(i\zeta) - \varepsilon_3(i\zeta)}{\varepsilon_1(i\zeta) + \varepsilon_3(i\zeta)} \right) \left( \frac{\varepsilon_2(i\zeta) - \varepsilon_3(i\zeta)}{\varepsilon_2(i\zeta) + \varepsilon_3(i\zeta)} \right) \end{aligned} \quad (2.34)$$

Since the frequency  $\zeta_1$  is usually large against contributions from molecular rotations, the dispersion term is mostly determined by electronic contributions. With a simple model for the electronic dielectric behaviour

$$\varepsilon(i\zeta) = 1 + \frac{n^2 - 1}{1 + \zeta^2/\zeta_e^2} \quad (2.35)$$

for each medium, where  $n$  is the index of refraction, the integration over the frequencies can be performed and one obtains a simplified formula containing only macroscopic quantities. It reads as

$$A = A_{n=0} + A_{n>0} \approx \frac{3}{4} kT \left( \frac{\varepsilon_1 - \varepsilon_3}{\varepsilon_1 + \varepsilon_3} \right) \left( \frac{\varepsilon_2 - \varepsilon_3}{\varepsilon_2 + \varepsilon_3} \right) + \frac{3\hbar\zeta_e}{8\sqrt{2}} F(n_1, n_2, n_3) \quad (2.36)$$

where

$$F(n_1, n_2, n_3) \equiv \frac{(n_1^2 - n_3^2)(n_2^2 - n_3^2)}{(n_1^2 + n_3^2)^{1/2}(n_2^2 + n_3^2)^{1/2}((n_1^2 + n_3^2)^{1/2} + (n_2^2 + n_3^2)^{1/2})}. \quad (2.37)$$

This formula shows that it is possible to tune the surface interactions by choosing surfaces with adequate dielectric behaviour and refractive indices such that the interaction terms, as a function of temperature, can show interesting behaviour: in

particular a change of sign, which then signals a change from favorable to unfavorable interactions, hallmark of a transition between two different states, favoring either wetting or dewetting.

A classification of the different types of forces that are ultimately of electrostatic origin, and their dependence on geometry, is given in the book by Israelachvili (1992).

## 2.3 Wetting and Dewetting: The Wetting Phase Diagram

The insights gained from the previous section now allow us to formulate the basic concepts of wetting beyond Young's equation, and in particular to address the notion of a *wetting (or dewetting) phase transition*. The basic mathematical object in this context is the *effective interface potential*  $V(h)$ . The notion *effective* in this context refers to the fact that this potential is not a microscopic potential, but that its parameters depend on temperature—e.g., via their indices of refraction, as shown in the previous section.

For large separations,  $h \rightarrow \infty$ ,  $V(h) \rightarrow 0$ , and in what follows we assume for the asymptotics for large separations a van der Waals interaction of the form

$$V(h) \sim \frac{A}{h^{m-1}}, \quad h \gg 0 \quad (2.38)$$

where we have collected the numerical factors into a redefined *Hamaker constant*  $A$  which we will use from now on. We call the exponent  $m$  in order to cover more general cases than the *non-retarded van der Waals forces*,  $m = 3$ , or the *retarded* van der Waals forces with  $m = 4$ ; also other values  $m > 1$  are possible. Even the (formal) case of  $m \rightarrow \infty$  is possible which we identify with exponentially decaying forces

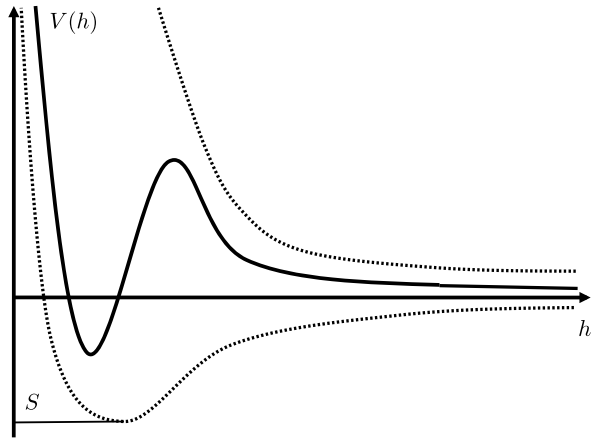
$$V(h) \sim \exp(-h/\xi) \quad (2.39)$$

with a decay length  $\xi$ . These forces correspond to short-ranged interactions between interfaces. The wetting phase transition was originally described in terms of the Ginzburg-Landau theory of phase transitions (Cahn 1977; Nakanishi and Fischer 1982) to which such forces apply.

Figure 2.9 shows three possible shapes the interface potential  $V(h)$  can display in the opposite limit  $h \rightarrow 0$ , i.e. close to the wall at which structural effects intervene (steric repulsion). These cases are

- a *stable thin film*: the force needed to push the two interfaces together continues to increase upon approach of the interfaces;
- an *unstable film*: the interfaces feel a strong attraction until a minimum is reached below which the force increases again. Note that, in this case, the Hamaker constant  $A < 0$ ;
- a *metastable film*: upon the approach of the two interfaces, the force first increases and then decreases before reaching a minimum. This is the typical behaviour

**Fig. 2.9** Schematic drawing of the effective interface potential  $V(h)$ . Three cases are depicted: *short dashes*: stable thin film; a thick film on this substrate would be unstable; *long dashes*: stable thick film; *solid line*: barrier separating a thin and a thick film state, with the relative stability being determined by the height difference between the two minima. In the case shown, the thin film is stable since  $S = V(h_{\min}) < 0$



expected when a free energy barrier needs to be surmounted. The relative position of the two minima in  $V(h)$  decides which is the metastable and which the stable state; in the potential shown, a microscopically thin film is stable on the surface, or an infinitely thick film.

The effective interface potential shown concerns the situation at chemical equilibrium, for which the chemical potential between the fluid phases is zero:  $\Delta\mu = 0$ . This, of course, need not be the case and we can therefore consider the more general full effective potential

$$\Phi(h) \equiv V(h) - (\Delta\mu)h. \quad (2.40)$$

$V(h)$  and  $\Phi(h)$  are compared for the case of a metastable state, again for the case for a metastable thick film in Fig. 2.10. The left figure shows a situation at coexistence with a stable thin film.

Figure 2.10 (right) displays the effective interface potential  $\Phi(h)$  in a situation in which a thick film is metastable on the wall. In the full interface potential  $\Phi(h)$  the minimum of  $V(h)$  at  $h = \infty$  is, for  $\Delta\mu < 0$ , shifted to a finite value  $h_1$ . Along a prewetting line the two minima of  $\Phi(h)$  have equal height, and they coincide at the prewetting critical point. The prewetting line is therefore the coexistence line of prewet and nonwet states.

For the case of an interface potential with a barrier, for which either the microscopically thin or the thick film state can be the metastable state, the corresponding thermodynamic states can be characterized by the generic wetting phase diagram shown in Fig. 2.11. This diagram fundamentally underlies all cases treated in this book; we will see in Chap. 3 different realizations in different physical systems. We denote the prewetting line in this text interchangeably as  $T_p(\Delta\mu)$  or, inversely, as  $\Delta\mu_p(T)$ , or  $\Delta\mu_p(S)$ . The spreading coefficient can be expressed in terms of temperature distance from the wetting transition  $W$ .

Figure 2.11 shows the phase diagram for a system which can have *first-order wetting transition* in terms of temperature  $T$  and chemical potential  $\mu$ . Above the

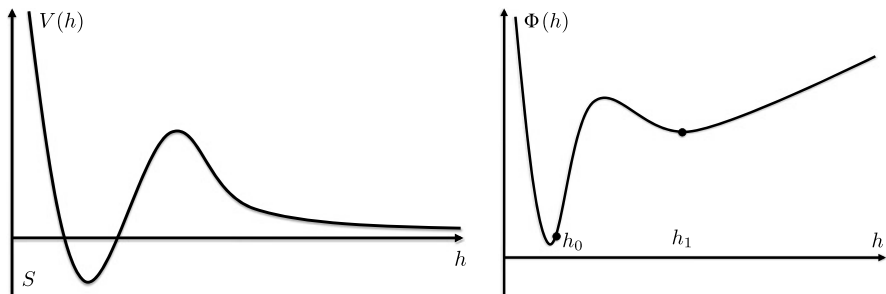


**Fig. 2.10** *Left*: The effective potential  $V(h)$ , where  $S \equiv V(h_{min})$  with the absolute minimum of  $V$  located at  $h_{min}$ ; *right*: the full potential  $\Phi(h) \equiv V(h) - (\Delta\mu)h$ . Here,  $h_1$  is the equilibrium thickness of the undercooled layer, and  $h_1 - h_0$  is the depth of the critical hole

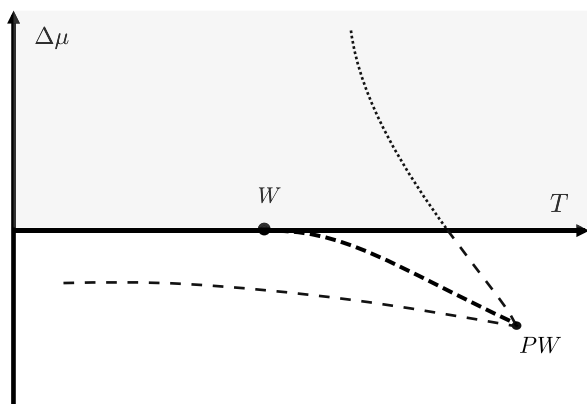


**Fig. 2.11** Generic wetting-dewetting phase diagram in the temperature-chemical potential plane. Indicated are the upper and lower surface spinodals (*thin dashed and dotted*), the first-order wetting transition point ( $W$ ), the prewetting line (*thick dashed*) and the prewetting critical point ( $PW$ ). The region above the coexistence curve is the bulk liquid side of the phase diagram (shown *shaded in gray*). The surface spinodal on the liquid side is indicated as a *dotted line* since the bulk liquid phase is stable on this side of the phase diagram

coexistence value  $\mu = \mu_c$  of the two-fluid bulk system the thickness of a wetting layer is infinite whereas for  $\Delta\mu \equiv \mu - \mu_c < 0$  it is finite. In the limit  $\Delta\mu \rightarrow 0$  from below the layer thickness diverges continuously above the wetting temperature  $T_w$  at  $W$ , but it has an infinite jump across the partial-wetting line  $T < T_w$ ,  $\Delta\mu = 0$ , reflecting the instability of the bulk phase. A finite jump from a thin to a thick layer occurs when the prewetting line  $T_p(\Delta\mu)$  is crossed from the region  $T < T_p(\Delta\mu)$  to  $T > T_p(\Delta\mu)$ . This jump runs to infinity when  $T_w$  is approached along the prewetting line, and it disappears at the prewetting critical point  $PW$ .

By contrast, for a system without a barrier, there is always only one minimum at  $\Delta\mu = 0$  which is either at a small, finite value of  $h$ , or at infinity. The phase transition between these two states occurs at a value  $T = T_c$ ,  $\Delta\mu = 0$  and is called a

*critical wetting transition*. It corresponds to the limit in which the prewetting critical point  $PW$  of Fig. 2.11 coincides with the wetting transition  $W$  at  $T = T_w$ . We will only briefly touch on this case in Chap. 3, but otherwise stay entirely away from the critical wetting case (which has a rich history in its treatment of fluctuation effects).

## 2.4 The Hamiltonian and the Line Tension

### 2.4.1 The Effective Interface Hamiltonian

We now have the two essential ingredients for a full mathematical interface model: the surface free energy from capillary theory, and the dispersion forces for ‘microscopic’—thin—films. We collect them together into the *effective interface Hamiltonian*

$$\mathcal{H}[h] = \int d^{d-1}x \left[ \frac{\sigma_{lv}}{2} (\sqrt{g} - 1) + V(h) - (\Delta\mu)h \right] \quad (2.41)$$

where  $\sqrt{g} = (1 + (\nabla h)^2)^{1/2}$ . We will mostly be interested in inhomogeneous states of the system (droplets and holes) and therefore have to study the variational problem

$$\frac{\delta \mathcal{H}[h]}{\delta h(x)} = 0 \quad (2.42)$$

which leads to a *nonlinear elliptic differential equation*

$$-\sigma_{lv} \nabla \left( \frac{\nabla h(x)}{\sqrt{g}} \right) + V'(h(x)) - \Delta\mu = 0. \quad (2.43)$$

What remains to be specified is the symmetry of the sought solution, as well as the proper boundary conditions.

We begin this study rightaway, for the case of the line tension. Our first task is to derive the *modified Young’s equation*, Eq. (2.12). We follow a discussion presented in Dobbs (1999a).

### 2.4.2 Line Tension I: The Modified Young Equation

We have seen before that the shape of the drop in the vicinity of the substrate deviates from the *dividing line* which is the macroscopic interpolation of the droplet profile down to the surface. Repeating the equation we have

$$\cos \theta_r = \cos \theta - \frac{\tau \kappa}{\sigma_{lv}} \quad (2.44)$$

where  $\theta$  is Young’s contact angle, determined by the surface tensions. We thus see that the real (or better *apparent contact angle*)  $\theta_r$  is determined by a superposition

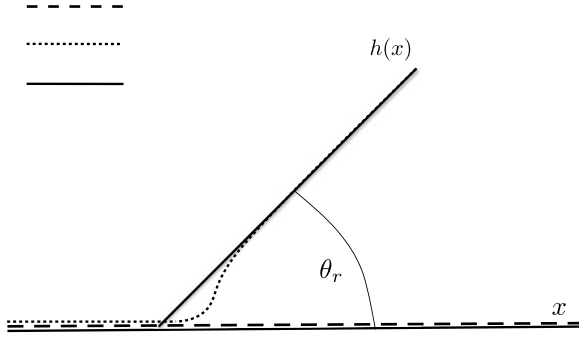


**Fig. 2.12** The foot of the droplet. *Drawn line*: macroscopic approximation; *dotted line*: proper profile for an interface potential corresponding to a first-order wetting transition which asymptotically approaches a film of thickness  $f$ ; *dashed line*: the thin film of thickness  $h_0$ , corresponding to the thin-film minimum of the interface potential  $V(h)$ . Adapted from Dobbs (1999a)

of an expression involving Young's contact angle  $\theta$  and a correction due to the line tension. It is thus tempting to identify this correction term as being generated by the interface potential, and we want to see exactly how that works, based on Eq. (2.41).

Assuming cylindrical symmetry of the drop, the profile has to obey the equation (2.43) in the form

$$\sigma_{lv} \left( \frac{dh}{dr} + \frac{1}{r} \right) \left( \frac{1}{\sqrt{g}} \frac{dh}{dr} \right) = V'(h(x)) - \Delta\mu. \quad (2.45)$$

In what follows, we normalize  $V_\sigma \equiv V/\sigma_{lv}$ ,  $(\Delta\mu)_\sigma \equiv \Delta\mu/\sigma_{lv}$ .

The boundary conditions to Eq. (2.45) are obviously at the center of the drop

$$h(0) = h, \quad h'(0) = 0 \quad (2.46)$$

while at infinity we must have a merging of the profile into a thin film of thickness  $f \approx h_0$ .<sup>3</sup> We suppose conditions of partial wetting ( $T < T_w$ ,  $\Delta\mu \approx 0$ ) with an interface potential exactly as in Fig. 2.10. For large values  $V(h)$  decays to zero. For convenience, however, we change our normalization and put the minimum of  $V(h)$  at the thin film to zero:  $V(h_0) = 0$ ; the potential then decays for large  $h$  to the value of the spreading coefficient,  $-S$ , noting that at partial wetting,  $S < 0$ . For the limit at large values of  $r$  one then has  $f - h_0 = \mathcal{O}((\Delta\mu)_\sigma)$ .

We have already seen that the macroscopic drop profile is determined by the chemical potential term; the Young equation part of Eq. (2.12) is thus assured. The apparent contact angle  $\theta_r$  is determined from the intersection of the dividing line from the droplet profile with the substrate surface which acts as a second dividing line, see Fig. 2.12.

<sup>3</sup>Note that for one-dimensional profiles,  $h_0 = h_{min}$ . This is not true for  $d > 1$  due to the appearance of a 'friction'-term in the ODE governing the interface profile: see the discussion in Sect. 2.5.

This identification allows to define a radius  $R$  and the contact angle  $\theta_r$  which are related to the chemical potential via

$$\Delta\mu R = 2\sigma_{lv} \sin \theta_r \quad (2.47)$$

and for the height of the drop one has

$$\Delta\mu(h - f) = 2\sigma_{lv}(1 - \cos \theta_r). \quad (2.48)$$

These relations generalize the previous relations (2.4) to the present case, including the effective interface potential.

We now expand the droplet shape in powers of  $1/R$  (or, more properly,  $\xi/R$  where  $\xi$  measures the radial extent on which the interface potential contributes, see Fig. 2.12). Only in the vicinity of the droplet edge the derivative of the interface potential dominates over the chemical potential difference in Eq. (2.45). To zeroth order, we therefore drop both  $(\Delta\mu)_\sigma$  and the term  $\sim 1/r$ . The remaining equation is then identical to that of a straight contact line with a first integral (Dobbs and Indekeu 1993) given by

$$\frac{1}{\sqrt{g}} \frac{dh}{dr} \approx -(2V_\sigma - V_\sigma^2)^{1/2}. \quad (2.49)$$

*Task: Verify Eq. (2.49).*

Likewise, one can integrate the full equation by using the relation

$$d/dr = (dh/dr)(d/dh). \quad (2.50)$$

With the boundary conditions at small and large  $r$  one finds the equation

$$V_\sigma(h) - V_\sigma(f) = \frac{(\Delta\mu)_\sigma}{2}(h - f) + \int_f^h d\tilde{h} \left( \frac{1}{r} \frac{h}{\sqrt{g}} + \frac{(\Delta\mu)_\sigma}{2} \right). \quad (2.51)$$

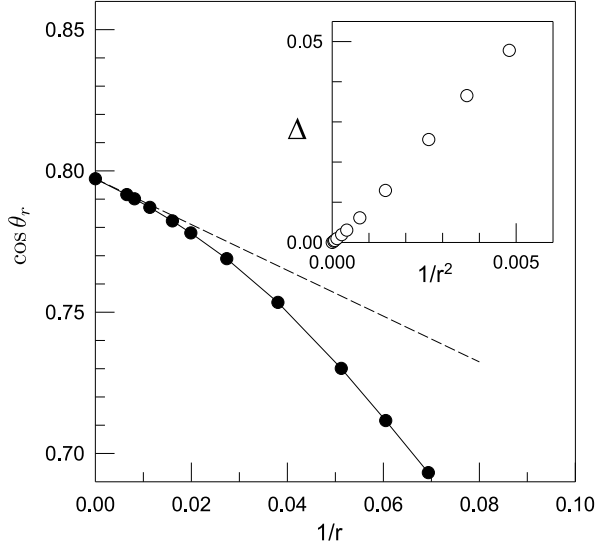
For large  $r$  the solution is given by the spherical drop and the integrand then tends to zero. Obviously, as stated before, the only region of interest is around  $f \approx h_0$  for which we can approximate the first term under the integral by the one-dimensional solution with  $r \approx R$ . Since  $(f - h_0) = \mathcal{O}(1/R)$  and  $V(f) = \mathcal{O}(1/R^2)$  one has, to first order:

$$V_\sigma(h) = \frac{(\Delta\mu)_\sigma}{2}(h - f) - \frac{1}{R} \int_{h_0}^h d\tilde{h} \left[ (2V_\sigma - V_\sigma^2)^{1/2} - \frac{(\Delta\mu)_\sigma}{2} R \right]. \quad (2.52)$$

If the intermolecular forces decay sufficiently rapidly, the interface potential can be approximated by its asymptotic behaviour for large  $r$ ,  $V(h) \approx S > 0$ , and the integral is convergent when the upper limit is taken to infinity. Then one obtains the modified Young equation: by using Eqs. (2.47), (2.48) and the definition of the spreading coefficient, we have

$$S = \sigma_{lv}(1 - \cos \theta_r) - \frac{\sigma_{lv}}{R} \int_{h_0}^\infty d\tilde{h} [(2V_\sigma - V_\sigma^2)^{1/2} - \sin \theta_r] \quad (2.53)$$

**Fig. 2.13** The *full line* and the *symbols* show the variation of  $\cos \theta_r$  with droplet radius  $R$ , numerically computed for a typical first-order wetting interface potential. The *dashed line* is the modified Young's equation with  $\tau$  given by Eq. (2.55). The *insert* shows the next-to-leading order correction. Reprinted with permission from Dobbs (1999a). Copyright by World Scientific



To lowest order, we replace the  $\sin \theta_r$ -term by  $\sin \theta$  and then obtain the *modified Young equation*

$$\cos \theta_r = \cos \theta - \frac{\tau}{\sigma_{lv} R} \quad (2.54)$$

with

$$\tau = \sqrt{2}\sigma_{lv} \int_{h_0}^{\infty} d\tilde{h} \left[ \left( V_{\sigma} - \frac{V_{\sigma}^2}{2} \right)^{1/2} - \left( (-S/\sigma_{lv}) - \frac{(-S/\sigma_{lv})^2}{2} \right)^{1/2} \right], \quad (2.55)$$

where we now use the non-renormalized expression for  $V$ . In the case of the squared-gradient approximation, this equation simplifies to

$$\tau = \sqrt{2}\sigma_{lv} \int_{h_0}^{\infty} d\tilde{h} \left[ V_{\sigma}^{1/2} - (-S/\sigma_{lv})^{1/2} \right]. \quad (2.56)$$

In Fig. 2.13, the variation of  $\cos \theta_r$  with radius  $R$  is shown from a numerical calculation making use of an exemplary interface potential corresponding to a first-order wetting case

$$V_{\sigma}(h) = Ae^{-(h-1)} + Be^{-2(h-1)} + Ce^{-3(h-1)} - S/\sigma_{lv} \quad (2.57)$$

with  $A = 3.3$ ,  $B = -7.0$ ,  $C = 3.5$ ,  $S/\sigma_{lv} = 0.203$ . The numerical result is compared to the modified Young equation with the line tension given by Eq. (2.55). Note that the plot is in  $1/R$ , and hence signals the deviation for smaller droplets. The next-to-leading order  $\Delta = \cos \theta - \tau/(\sigma_{lv} R) - \cos \theta_r$  is in  $1/R^2$ , as seen in the inset in Fig. 2.13.

We close this discussion with remarks on the limit in Eq. (2.55). One finds that the reasoning is only correct provided  $m \geq 3$ , i.e., in presence of retarded and non-retarded van der Waals forces. For still longer-ranged forces,  $2 < m < 3$ , the inte-

gral is still convergent, but the next-order term behaves according to  $R^{-(m-1)}$ . For  $m \leq 2$ , the integral diverges and molecular details then need to be considered.

### 2.4.3 Line Tension II: The Elasticity of the Contact Line

In this section we look at the (elastic) response of the localized interface to a local distortion. If we try to enlarge a flat liquid interface, we have to pay a price in surface free energy which is proportional to the surface tension. When we disturb the line, we might again expect to run into a line tension. Is this so—and is this object related to the line tension we discussed so far? Again, we follow a discussion presented by Dobbs (1999b). We expect that the *work per unit length*  $\delta\mathcal{H}$  can be written as a quadratic function of the amplitudes

$$\delta\mathcal{H}(q) = \frac{1}{2} W(q) \eta_q^2 \quad (2.58)$$

where the  $\eta_q$  are Fourier coefficients. Our interest is in the function  $W(q)$ .

We address this problem by assuming as the starting point a one-dimensional interface profile in  $x$ -direction which is translationally invariant in  $y$ -direction. The effective interface Hamiltonian reads as

$$\mathcal{H}[h] = \frac{1}{L_y} \int dx dy \left[ \frac{\sigma_{lv}}{2} (\nabla h)^2 + V(h) \right] \quad (2.59)$$

at coexistence,  $\Delta\mu = 0$ . Without a distortion, the interface profile fulfills the variational equation

$$\frac{\sigma_{lv}}{2} h'(x)^2 = V(h) \quad (2.60)$$

and we assume the boundary condition  $h(x) \rightarrow h_0$  for  $x \rightarrow -\infty$ . For  $x \rightarrow \infty$ , the profile grows monotonously with the limiting behaviour for  $h \rightarrow \infty$  as  $\sigma_{lv} (\tan \theta)^2 = -2S$ , with  $S < 0$  at partial wetting.

In order to determine the ‘line tension’ associated with this configuration we have to introduce the dividing line again, but since we are now looking at an unbounded profile in one direction, we have to modify our expressions accordingly. We use the following form for the harmonic approximation

$$\tau = \sqrt{2\sigma_{lv}} \int_{h_0}^{\infty} dh [V(h)^{1/2} - (-S)^{1/2}]. \quad (2.61)$$

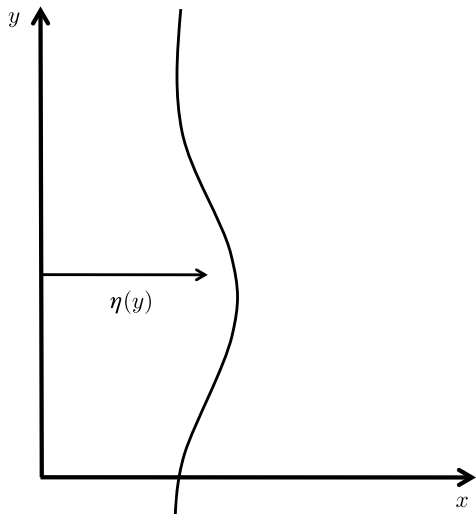
Distorting the line according to

$$h(x, y) = h(x) + \xi(x, y) \quad (2.62)$$

we can obtain a quadratic expression in  $\xi$ :

$$\delta\mathcal{H}^{(2)} \equiv \frac{1}{L_y} \int dx dy \xi(x, y) [-\sigma_{lv} \nabla^2 + V''(h(x))] \xi(x, y), \quad (2.63)$$

**Fig. 2.14** Local translation of the interface



where the effective potential term now contains the whole interfacial profile. The expression in brackets

$$\mathcal{M} \equiv [-\sigma_{lv} \nabla^2 + V''(h(x))] \quad (2.64)$$

looks like a *Schrödinger operator* of a two-dimensional Hamiltonian. Figure 2.15 displays the interfacial profile, the potential and the ground state wave function to this operator. An eigenstate of the Hamiltonian is easily obtained, as it is the translational mode

$$\phi_0(x) = h'(x) \quad (2.65)$$

which has the eigenvalue zero. The fact that the ground state has eigenvalue zero proves the stability of the configuration;  $W(q) > 0$  for any wavenumber  $q$ .

*Task: Show explicitly that  $\phi_0$  is an eigenstate to the operator  $\mathcal{M}$  in Eq. (2.63) with eigenvalue zero.*

We now enter a subtle point, marking a difference between the case of an interface between two homogeneous phases, like in bulk, or at the prewetting transition in the case of interfaces. In order to derive  $W(q)$  we would then consider local translations, see Fig. 2.14

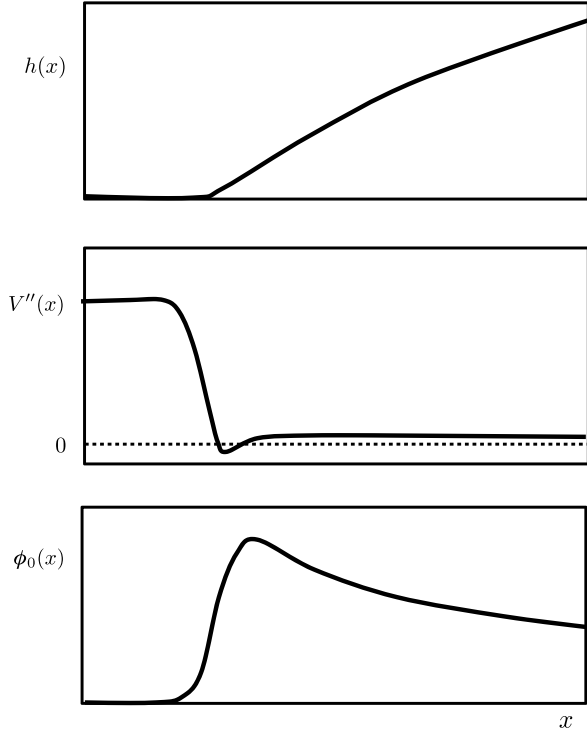
$$h(x, y) = h(x - \eta(y)) \quad (2.66)$$

and we were to obtain

$$W(q) = \frac{\sigma_{lv}}{2} q^2 \int_{-\infty}^{\infty} dx \phi_0^2. \quad (2.67)$$

In the present case, this reasoning does not hold because the integral does not converge in the case of a contact line at partial wetting since  $\phi_0(x)$  tends to  $\sim \tan \theta$  on one side far away from the contact line and therefore the integral diverges. We

**Fig. 2.15** The interface profile  $h(x)$ , the potential  $d^2 V/dh^2(h(x)) \equiv V''(x)$  and the (non-normalized) ‘ground state wavefunction’  $\phi_0(x)$  for the exemplary interface potential  $V(h) = h^2/(h+1)^4$ . For large  $x$ ,  $h \sim \sqrt{x}$ , while  $\phi_0(x) \sim x^{-1/2}$ . The potential  $V''(x)$  has a very broad (undiscernable) maximum at  $x = 6.8$  and decays to zero for large  $x$  from above. Adapted from Dobbs (1999b)



thus have to introduce a constraint in order to render the calculation mathematically meaningful.

If we call  $x_c$  the position of the undistorted line,  $h(x_c) = h_c$ , the displacement of the distorted line is given by

$$\eta(y) \equiv -\xi(x_c, y)/\phi_0(x_c) \quad (2.68)$$

to first order in  $\xi$ . This corresponds to measuring the displacement with respect to a particular value of a ‘level-set’ introduced by  $h_c$ . With the choice of a periodic distortion

$$\xi(x, y) = -\eta_q \phi_q(x) \sin(qy) \quad (2.69)$$

the function  $\phi_q(x)$  must then satisfy

$$\phi_q(x_c) = \phi_0(x_c). \quad (2.70)$$

Inserting the expression (2.69) into the expression for  $W(q)$  one obtains after integration over  $y$  the dispersion relation

$$W(q) = \frac{1}{2} \int_{-\infty}^{\infty} dx \phi_q(x) \left[ -\sigma_{lv} \left( \frac{d^2}{dx^2} - q^2 \right) + V''(h(x)) \right] \phi_q(x). \quad (2.71)$$

We now minimize this integral with respect to  $\phi_q$  under the constraint (2.70), which we perform by adding a corresponding term with a Lagrange multiplier  $\lambda_q$ . The resulting Euler-Lagrange equation is

$$\left[ -\sigma_{lv} \left( \frac{d^2}{dx^2} - q^2 \right) + V''(h(x)) \right] \phi_q(x) = \lambda_q \delta(x - x_c) \quad (2.72)$$

with the  $\delta$ -function  $\delta(x - x_c)$ . While in the standard case we could approximate  $\phi_q$  with its ground state  $\phi_0$  to simply have Eq. (2.67), in the present case we have to really determine  $\phi_q(x)$ . The reason is that the approximation by the ground state fails since in the standard case there is a gap between the ground state and the lowest excited state while in our case there is a continuum of states lying above the ground state.

The states  $\phi_q(x)$  can be calculated from a WKB-based matching analysis. Details can be found in Dobbs (1999b); we here only sketch the solution.<sup>4</sup> First, the solution is divided into an ‘inner’ and an ‘outer’ region whose matching point  $x_m$  is defined by the condition

$$\frac{d}{dx} (V''(h(x)/\sigma_{lv}) \approx (q^2 + V''/\sigma_{lv})^{3/2}. \quad (2.73)$$

In the outer region  $x > x_m$  a WKB-approximation yields  $\phi_q(x) \sim \exp(-qx)$ . In the inner region the potential  $V''$  varies rapidly and the WKB-approximation fails. Instead, one writes

$$\phi_q(x) = \phi_0(x) e^{-S(x)} \quad (2.74)$$

where the function  $S(x)$  is continuous at  $x_c$ , and  $S(x_c) = 0$ . The jump in derivative at  $x_m$  is proportional to  $\lambda_q$ .  $S(x)$  fulfills a second-order differential equation which can be solved in an expansion in wavevectors. One finds

$$S(x) = \begin{cases} \mathcal{O}(q^2), & x < x_c \\ a(q) \int_{x_c}^x d\tilde{x} \phi_0^{-2}(\tilde{x}) & x_c < x < x_m \end{cases} \quad (2.75)$$

which matches the outer solution

$$\phi_q(x) = \phi_0(x_m) e^{-S(x_m) - q(x - x_m)} \quad (2.76)$$

where  $a(q) \approx q(\tan \theta)^2$  for partial wetting, and of higher order in  $q$  at wetting. In sum, one finds for  $W(q)$

$$W(q) = \frac{\sigma_{lv}}{2} (\tan \theta)^2 |q| + \frac{\tilde{\tau}}{2} q^2 + \mathcal{O}(|q|^3), \quad (2.77)$$

with

$$\tilde{\tau}(S) = \sqrt{2\sigma_{lv}} \int_{h_0}^{\infty} dh [V^{1/2} - \Theta(h - h_c) S^2 V^{-3/2}], \quad (2.78)$$

---

<sup>4</sup>We will encounter this kind of matching procedure also in Part II of the book in the discussion of dynamic interface profiles.

which in general *differs* from the expression for the line tension, Eq. (2.56). This obviously reflects the nature of the imposed deformation and it also makes clear that in an experimenter has to be careful what quantity is actually looked at.

It is particularly noteworthy that this result depends on the *choice of the position of the contact line*,  $h_c = h(x_c)$ . This is true at partial wetting, as the result shows, while for  $S = 0$ , i.e. at wetting,  $\tau$  and  $\tilde{\tau}$  coincide. The approach to the wetting point goes for both expressions with the same power-law dependence in  $S$ , but with different amplitudes. The linear  $|q|$ -dependence is a classic result, see de Gennes (1985).

From the results in this and in the previous section we have learned the first facts about of spatially varying solutions to the (augmented) Young-Laplace equation. In particular, we have clarified the previous purely phenomenological results on the modified Young-equation and learned more about the properties of the line tension at partial wetting, and it also clarifies the interpretation of the experiments on line tensions, as described in Sect. 2.1. There we had also realized that the associated characteristic scales are on the order of 1 nm, hence a truly microscopic length scale. This immediately limits the usefulness and applicability to our interface-model approach, and leaves room for more microscopic approaches, like density-functional theory. We will come to this approach briefly in the next chapter and here only point to recent work by Weijs et al. (2011) describing a study of the line tension combining Molecular Dynamics (MD) simulations and density-functional theory (DFT).

We now turn to a detailed discussion of the *metastable states* that can be identified in the phase diagram of Fig. 2.16, based on the interface potential approach.

## 2.5 Characterizing Metastable Thin Films

In this section we discuss the properties of one kind of nonequilibrium wetting states which are *metastable states*. Such states are transient states which arise when, briefly stated, the following conditions are met:

- the effective interface potential has a barrier separating a thin from a thick equilibrium state as in Fig. 2.9;
- if  $S > 0$  and a thin film is overheated from below to above the prewetting line;
- if  $S < 0$  and a thick film is undercooled to below the prewetting line.

In the case  $S > 0$ , the thin film minimum lies energetically above the thick film minimum, while the opposite is the case for  $S < 0$ . For  $S > 0$ , the thin film has thus become a thermodynamically metastable state since it is still locally confined to a parabolic potential, however it has become *globally unstable*. Its confinement to a local parabolic potential, however, does not render it unstable to simple Gaussian fluctuations. A *nonlinear fluctuation* must arise, and in the case of a metastable thin film, this is a droplet of the liquid phase. It must reach a critical free energy (or, simply, *size*) to be able to surmount the free energy barrier between the two states.

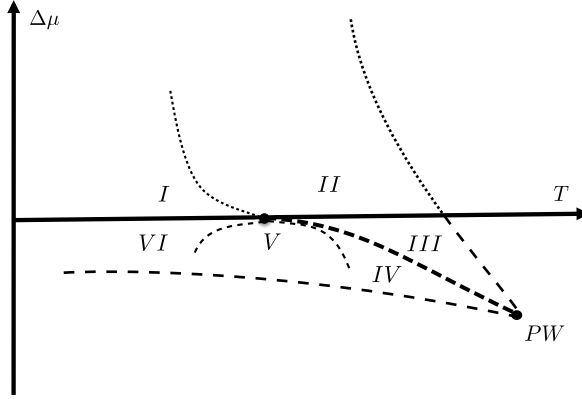


**Fig. 2.16** Wetting-dewetting phase diagram in the temperature-chemical potential plane. Indicated are the upper and lower surface spinodals (*thin dashed* and *dotted*), the first-order wetting transition point ( $W$ ), the prewetting line (*thick dashed*) and the prewetting critical point ( $PW$ ). The roman numerals I–VI indicate different scaling regimes of the critical nuclei (droplet and holes) in the phase diagram and are discussed in detail in the text

This critical free energy is, precisely, the *excess free energy* of a *critical droplet*. The critical droplet, and by analogy the *critical hole*, are thus *the essential objects* to characterize a first-order wetting/dewetting transition since the nucleation rate is given by the expression

$$I = D_0 A_0 \exp - \frac{E_c}{k_B T} \quad (2.79)$$

where  $D_0$  is a prefactor depending on the dynamics of the system, while  $A_0$  is a static prefactor determined by the Gaussian fluctuations of the critical droplet or hole. The inverse of the nucleation rate is the lifetime of the metastable state.

Our starting point for the calculation of the properties of the critical droplet as well as the critical hole is yet again the effective interface Hamiltonian—as we already used it before, but we now only consider the version with a linearized capillary term,

$$\mathcal{H}[h] = \int d^{d-1}x \left[ \frac{\sigma_{lv}}{2} (\nabla h)^2 + V(h) - (\Delta\mu)h \right]. \quad (2.80)$$

This simplification is warranted here since we will be only interested in the *scaling behaviours* of the droplet and hole geometry and the excess free energy in the vicinity of coexistence lines. For the metastable wetting and dewetting states the critical nucleus is again determined by the variational problem

$$\frac{\delta \mathcal{H}[h(r)]}{\delta h(r)} = 0 \quad (2.81)$$

which leads to the nonlinear elliptic differential equation

$$-\sigma_{lv} \Delta_r h(r) + V'(h(r)) - \Delta\mu = 0, \quad (2.82)$$

where  $\Delta_r$  now is the cylindrical Laplace operator (the radial Laplacian in two dimensions). The critical droplet and critical hole solutions to Eq. (2.82) correspond to two different sets of boundary conditions. We now discuss both types of solutions.

The different possible configurations of critical droplets and critical holes can more precisely be discussed in the context of the wetting phase diagram which allows us to delimit the regions of metastability, see Fig. 2.16. A metastable wetting state can be generated by overheating a microscopically thin layer from  $T < T_p(\Delta\mu)$  into a nucleation region bounded by  $T_p(\Delta\mu)$  and an *upper spinodal line*  $T_{us}(\Delta\mu)$ . The spinodal line is determined by the condition  $V'(h) - \Delta\mu = V''(h) = 0$ . The transition to the stable thick-layer configuration occurs via the random formation of droplets on the thin layer and the growth of supercritical droplets. Close to the prewetting line the critical droplets have a cylindrical shape with a diverging radius at  $T_p(\Delta\mu)$ . This had already been pointed out early on by Joanny and de Gennes who chose the name ‘pancake droplets’ for this type of critical nuclei (Brochard-Wyart et al. 1991; Joanny and de Gennes 1984). For critical holes, in total three distinct scaling regimes exist: partial wetting (I), complete wetting (II) and prewetting (III), as we will see.

Dewetting by nucleation of holes can occur when a thick wetting layer from  $T > T_p(\Delta\mu)$  is undercooled into a second nucleation region located between  $T_p(\Delta\mu)$  and a *lower spinodal line*  $T_{ls}(\Delta\mu)$ . In this case the critical nuclei are holes in the layer which near  $T_p(\Delta\mu)$  are mirror images of the pancake droplets. As we will see, however, close to the partial-wetting line the critical holes have a funnel-like profile with a diverging depth  $H_c$  but a finite inner radius  $R_c$  at  $\Delta\mu = 0$ . There exists a third regime, adjacent to the wetting transition point  $T = T_w$ ,  $\Delta\mu = 0$ , at which  $H_c$  and  $R_c$  both diverge. We refer to these regimes as the pre-dewetting regime (IV), the complete dewetting regime (V), and the partial-dewetting regime (VI). The three scaling regimes for the critical holes mirror the scaling regimes for the critical droplets.

### 2.5.1 Wetting by Nucleation: The Critical Droplet

We first discuss the existence of critical droplet solutions, i.e. solutions to Eq. (2.82) which fulfill the boundary conditions (see the sketch in Figs. 2.17, 2.18)

$$h'(0) = 0, \quad h(\infty) = h_0 \quad (2.83)$$

where  $h_0$  is the thickness of the thin film state, i.e., the microscopic film on the substrate.

An existence proof for a critical droplet solution to Eq. (2.82) is easily sketched by a mechanical analogy based on argument originally made by Sidney Coleman in the context of bulk nucleation (Coleman 1985) and was applied to wetting in Bausch and Blossey (1991). The argument can also be made rigorous (Berestycki

et al. 1981). First we make use, as for the mesoscopic droplet we discussed at the beginning of the chapter, of the cylindrical symmetry of the droplet and then have

$$-\sigma_{lv} \left( h''(r) + \frac{d-2}{r} h'(r) \right) + V'(h(r)) - \Delta\mu = 0. \quad (2.84)$$

In the mechanical analogy one interprets the variational equation (2.84) as an equation of motion of a classical particle in time  $t \equiv r$  moving in the inverted potential  $W(h) = -\Phi(h)$ . The potential then has a typical double-well structure for a finite chemical potential difference, or a very asymmetric shape with one minimum shifted to  $+\infty$  if  $\Delta\mu = 0$ , i.e. at coexistence of the two bulk phases. Let us first consider this case.

The solution is obtained if an initial value  $h_c$  is found such that for  $r \rightarrow \infty$  the solution reaches the maximum of  $W(h)$  at  $h = h_0$ . This solution is the unique case limiting two other types of solutions, whose existence is readily established. If we start a solution ‘far out’ from the maximum (large  $h_c$ ), and still away from local minimum, the solution will spend a long time in the fairly flat region of the potential, and still be at a point for which  $W(h) > W(h_0)$ . Since the time-dependent friction term  $\sim 1/r$  by then has become very small, it can then be neglected and the remaining potential energy of the solution will lead the particle to overshoot the maximum. On the other hand, if we start the particle such that  $W(h_1) = W(h_0)$ , the friction term suffices to turn the solution into an oscillatory, undershooting solution which ends up in the minimum of  $W(h)$ . The physical solution is the limiting one between the undershooting and overshooting solutions.

In the case  $\Delta\mu \neq 0$ , the same reasoning holds; only now an overshooting solution is constructed by placing the starting point for the solution close to the thick-film maximum. Then again the solution spends a long time in the vicinity of the maximum so that the friction-term can be neglected in its further motion.

Based on the behaviour of these limiting solutions in the different regions of the wetting phase diagram we can quantify the three scaling regimes for critical droplets (I–III in Fig. 2.16) as follows.

- *Partial wetting.* If the wall of the system is brought from the gaseous phase to the liquid phase (from  $\Delta\mu < 0$  to  $\Delta\mu > 0$ ), droplets condense at the wall. This is the classic case of *heterogeneous nucleation* at a wall (Blossey 1995). A droplet sitting at the wall simply has less volume than a critical droplet in the bulk, and hence nucleation at the wall is favoured. In our system, this is the case on the liquid side of the bulk phase diagram,  $\Delta\mu \rightarrow +0$ , for temperature  $T < T_w$ . These droplets essentially are a generalization of the droplets discussed at the beginning of this chapter. Since we kept the dependence on spatial dimension in our formula (2.84)—an approach learnt from the theory of phase transitions—we obtain the general results for the height of the critical droplet  $H_c$ , its radius  $R_c$  and the excess free energy  $E_c$  (Bausch and Blossey 1993):

$$H_c = (d-1) \frac{|S|}{\Delta\mu}, \quad R_c = (d-1) \sqrt{2\sigma_{lv}} \frac{|S|^{1/2}}{\Delta\mu} \quad (2.85)$$

**Fig. 2.17** Sketch of the radial profile of a critical droplet

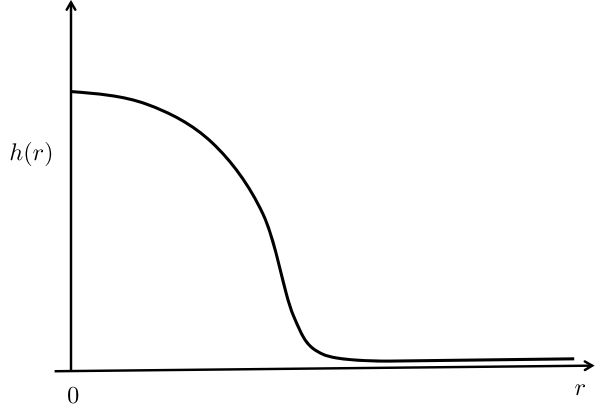
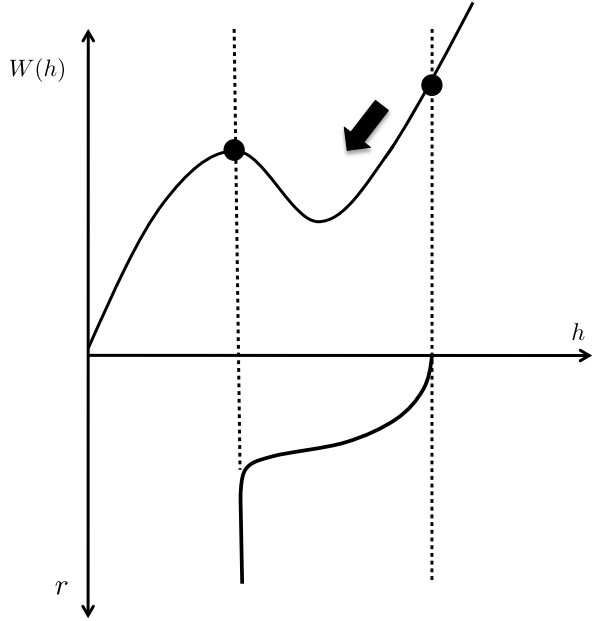


**Fig. 2.18** Construction of the droplet solution. For the explanation, see text



and

$$E_c = \Omega_{d-1} 2^{(d+1)/2} \sigma_{lv}^{(d-1)/2} \frac{(d-1)^{d-2}}{d+1} \frac{|S|^{(d+1)/2}}{(\Delta\mu)^{1-d}} \quad (2.86)$$

where  $\Omega_{d-1}$  is the surface of the  $(d-1)$ -dimensional unit sphere.

- *Complete wetting.* Here, the droplets are found to scale according to

$$R_c \sim H_c^{(m+1)/2} \quad (2.87)$$

and

$$E_c \sim R_c^{d-2} \ln R_c \quad (2.88)$$

for  $m = 3$ , non-retarded van der Waals forces, and

$$E_c \sim R_c^{d-2} \quad (2.89)$$

if the forces fall off more rapidly,  $m > 3$ .

- *Prewetting*. In the vicinity of the prewetting line, the droplets are pancake-like (as stated before) with a scaling behaviour

$$R_c \sim [\Delta\mu - \Delta\mu_p(S)]^{-1} \quad (2.90)$$

and

$$E_c \sim [\Delta\mu - \Delta\mu_p(S)]^{2-d} \quad (2.91)$$

where  $\Delta\mu_p(S)$  is the prewetting line.

The appearance of logarithmic corrections in the scaling behaviour of critical droplets was noted by Joanny and de Gennes (1984). The paper by Bausch and Blossey (1993) accounts for the full scaling theory of critical droplets at first-order wetting phase transitions, including the crossover between the three scaling regimes, a point we do not pursue here.

The approach also allows to determine the line tension of the drop, which allows to make contact with our previous discussion. At coexistence it scales upon approaching the wetting transition point according to

$$\tau \sim \begin{cases} |S|^{(m-3)/[2(m-1)]} & m < 3 \\ \ln |S| & m = 3 \\ \text{const.} & m > 3. \end{cases} \quad (2.92)$$

We see that for  $m < 3$  the line tension  $\tau$  diverges as  $S \rightarrow 0$ , i.e., at complete wetting. This divergence has played a (rather confusing) role in the interpretation of experimental results of dewetting experiments in helium films, see Chap. 3.

This brings us to the properties of critical holes.

### 2.5.2 Dewetting by Nucleation: The Critical Hole

The link between a bulk-controlled nucleation regime at low temperatures and a surface-dominated nucleation regime above the wetting temperature gives the nucleation phenomenon at wetting already a much richer phenomenology than is the usual case. The specific geometry of the wetting phase diagram has another peculiar feature which shows up in the behaviour of undercooled films. While droplet nucleation is conceptually fairly similar to droplet nucleation in the bulk, hole nucleation is very different (Bausch and Blossey 1994).

The reason for this is very easily understood by a simple consideration of the path of undercooling, and the lines it crosses in the wetting phase diagram, see Fig. 2.19.

Starting point is a stable thick film at an interior point of the prewetting region of the phase diagram close to bulk coexistence, but of course on the gas side. Undercooling this film puts it on a trajectory which crosses the prewetting line and then

**Fig. 2.19** A typical undercooling path of a thick film to below the prewetting line

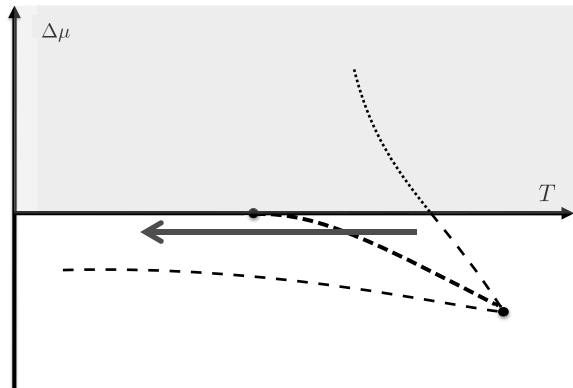
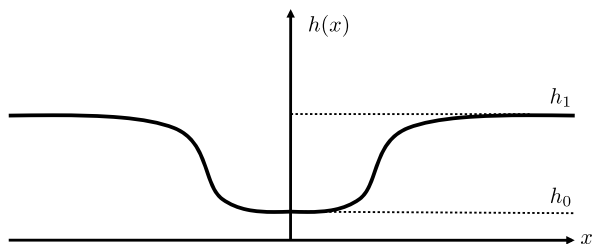


**Fig. 2.20** Schematic sketch of the radial profile of a critical hole



continues on to well below the wetting temperature  $T_w$ . The final destination thus is a point close to bulk coexistence,  $\mu \approx \mu_c$ . Near bulk coexistence at  $T < T_w$ , the size of critical nuclei and their excess free diverge.

The critical holes will have peculiar properties, which we now deduce. The approach follows Foltin et al. (1997). In order to do this, we first specify the two boundary conditions to equation (2.84). They are, see Fig. 2.20

$$h'(r=0) = 0, \quad h(r=\infty) = h_1 \quad (2.93)$$

where  $h_1$  is the film thickness of the flat film at infinity. We note that for the case at coexistence,  $\Delta\mu = 0$ ,  $h_1(\infty) = \infty$  is allowed (and is related to the peculiarity of the critical hole).

As for the critical droplets, we can argue for the existence of critical holes in the vicinity of the prewetting line with the shooting argument presented above. Near interior points of the prewetting line the potential  $\Phi(h)$  has a double-well form which for the radial profile of a critical hole leads to a kink solution. In the limit  $T \rightarrow T_p(\Delta\mu)$  the position  $R_c$  of the turning point of the kink runs to infinity, resembling the behaviour of a pancake droplet.

However, when some point on the line  $\Delta\mu = 0$ ,  $T \leq T_w$  is approached,  $h_1$  and the critical hole depth  $H_c \equiv h_1 - h_0$  diverge. In this regime the critical-hole profile at macroscopic distances from the wall is determined by the asymptotic behaviour of  $V(h)$  for  $h \rightarrow \infty$ . For long-range molecular interactions this is, as we have seen before,

$$V(h) = Ah^{1-m}, \quad \text{for } m > 1 \quad (2.94)$$

where  $A$  is the (redefined) Hamaker constant, and  $m = 3$  or  $m = 4$  for non-retarded or retarded van der Waals forces, respectively. By extrapolation the macroscopic profile  $H(r)$  of a critical hole can then be defined as the solution of the differential equation

$$\sigma_{lv} \left( H''(r) + \frac{d-2}{r} H'(r) \right) = -A(m-1)H^{-m} - \Delta\mu \quad (2.95)$$

with the new boundary conditions  $H(r = R_c) = 0$  and  $H(r = \infty) = h_1$  at  $\Delta\mu < 0$  or  $H'(r = \infty) = 0$  at  $\Delta\mu = 0$ , respectively. Undershooting and overshooting solutions can still be created, but now by controlling the initial velocity  $H'(r = R_c)$ .

Since for  $r \rightarrow R_c$  the friction term and the field  $\Delta\mu$  can be neglected in Eq. (2.95), one obtains the analytical result

$$H(r) = \left[ \frac{A}{2\sigma_{lv}}(m+1)^2 \right]^{\frac{1}{m+1}} (r - R_c)^{\frac{2}{m+1}} \quad (2.96)$$

which is asymptotically valid for all  $\Delta\mu \leq 0$ .

For  $r \rightarrow \infty$  and  $\Delta\mu \neq 0$  a linear expansion of Eq. (2.95) in  $(H_c - H(r))$  leads to a Bessel-type differential equation. This implies an asymptotic form

$$H(r) = H_c \left[ 1 - C \left( \frac{r}{R^*} \right)^{\frac{2-d}{2}} e^{-r/R^*} \right] \quad (2.97)$$

where  $R^* \equiv [Am(m-1)/\sigma_{lv}]^{-1/2} H_c^{(m+1)/2}$ , and  $C$  is an integration constant. If, as an approximation to the full solution of Eq. (2.95), the expressions (2.96) and (2.97) and their derivatives are matched at some value  $r = R_m$ , it turns out that  $R_m \sim R^*$  and the constant  $C$  is of order 1.

For  $r \rightarrow \infty$  and  $\Delta\mu = 0$  the left-hand side in Eq. (2.95) dominates for dimensions  $d < d_1(m)$  where the dimension  $d_1(m)$  is defined by

$$d_1(m) \equiv \frac{3m+1}{m+1}. \quad (2.98)$$

This leads to the behaviour

$$H(r) = H^* D \left( \frac{r}{R_c} \right)^{3-d} \quad (2.99)$$

for the critical hole profile. Here, the amplitude

$$H^* \equiv [A(m+1)^2/8\sigma_{lv}]^{1/(m+1)} R_c^{2/(m+1)} \quad (2.100)$$

has been adopted from the exact solution<sup>5</sup>

$$\left( \frac{r}{R_c} \right)^2 - \left( \frac{H}{H^*} \right)^{\frac{m+1}{2}} = 1 \quad (2.101)$$

<sup>5</sup>Note that the solution with the '+'-sign corresponds indeed to a droplet solution in the same dimension,  $d = d_0(m)$ : (Bausch et al. 1994).

of Eq. (2.95) at  $\Delta\mu = 0$  in the special dimension

$$d_0(m) \equiv \frac{3m-1}{m+1}, \quad (2.102)$$

so that  $D = 1$  in  $d = d_0(m)$ .

Due to the boundary condition  $H'(r = \infty) = 0$  the asymptotic form (2.99) implies that critical holes at  $\Delta\mu = 0$  only exist in dimensions  $d > 2$ . The necessity of the previously mentioned additional condition  $d < d_1(m)$  will become clear through the following analysis in which we map the ordinary differential equation of second order for the droplet profile to a dynamical system.

### 2.5.3 Mapping to a Dynamical System

Further insight into the solutions can be gained by mapping the ODE to a system of first-order equations, with the peculiarity that, for  $\Delta\mu \neq 0$ , the system can be represented by three equations. This transformation was conceived by G. Foltin; for the original treatment, which we closely follow, see Foltin et al. (1997).

We define the dimensionless quantities

$$\begin{aligned} X &\equiv \frac{r H'(r)}{H(r)}, \\ Y &\equiv \left( \frac{m^2 - 1}{2} \right) \frac{A}{\sigma_{lv}} \frac{r^2}{H^{m+1}(r)}, \\ Z &\equiv -\frac{1}{2} \frac{\Delta\mu}{\sigma_{lv}} \frac{r^2}{H(r)}, \end{aligned} \quad (2.103)$$

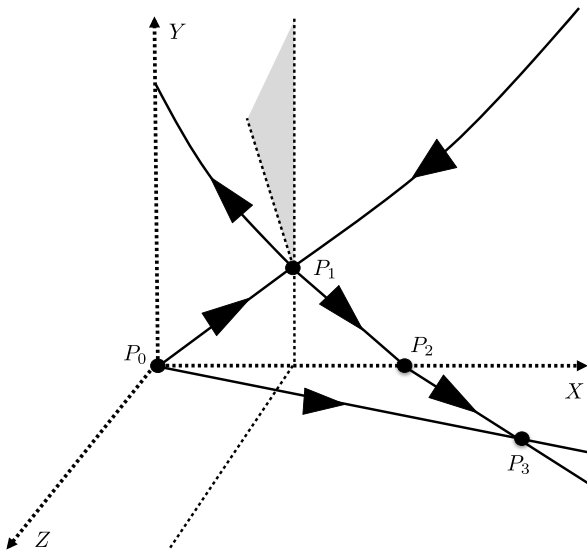
and consider their dependence on the time-like variable

$$t \equiv \ln\left(\frac{r}{r_1}\right) \quad (2.104)$$

where  $r_1$  is an arbitrary reference scale. Due to (2.4) we find the set of first-order ordinary differential equations in  $(X, Y, Z)$ ,

$$\begin{aligned} \dot{X} &= (3-d)X - X^2 - \frac{2}{m+1}Y + 2Z, \\ \dot{Y} &= 2Y \left( 1 - \frac{m+1}{2}X \right), \\ \dot{Z} &= 2Z \left( 1 - \frac{1}{2}X \right). \end{aligned} \quad (2.105)$$

**Fig. 2.21** The flow diagram of the dynamical system (2.105) with all fixed points and their principal directions. The shaded region is the sector in the plane  $X = 2/(m+1)$  penetrated by the physical trajectories for  $\Delta\mu < 0$ ; redrawn after (Foltin et al. 1997)



This system has four fixed points

$$\begin{aligned}
 X_0 = Y_0 = Z_0 &= 0, \\
 X_1 &= \frac{2}{m+1}, & Y_1 &= d_1(m) - d, & Z_1 &= 0, \\
 X_2 &= 3 - d, & Y_2 &= Z_2 = 0, \\
 X_3 &= 2, & Y_3 &= 0, & Z_3 &= d - 1,
 \end{aligned} \tag{2.106}$$

and we will now discuss their properties.

For  $1 < d < d_1(m)$  the fixed points (2.106) are all located in the octant  $X \geq 0$ ,  $Y \geq 0$ ,  $Z \geq 0$ , where the critical-hole trajectories occur (whereas  $H'(r) \leq 0$  implies  $X \leq 0$  for critical droplets). The subscripts of the fixed-point coordinates indicate the numbers of the attractive principal directions of each of these points.

In the plane  $Z = 0$  the fixed point  $P_1$  in Fig. 2.21 attracts the physical trajectories coming from  $X = Y = \infty$  which then either run to the droplet region  $X < 0$ , or to the more stable fixed point  $P_2$ . The first possibility corresponds to undershooting solutions of the saddle-point equation, whereas the second one describes solutions that obey the boundary conditions for critical holes at  $\Delta\mu = 0$ . The fixed-point value  $X_2 = 3 - d$  in connection with the definition of  $X$  reproduces the asymptotic behaviour (2.99) up to an undetermined prefactor. In the limit  $d \rightarrow d_1(m)$  the fixed point  $P_1$  merges into  $P_2$ , and in Fig. 2.21 the right section of the basin of attraction of  $P_2$  collapses to zero so that critical holes at  $\Delta\mu = 0$  no longer exist for  $d > d_1(m)$ .

If  $\Delta\mu < 0$ , the physical trajectories approach  $P_1$  from  $X = Y = Z = \infty$  but now have three options to continue. Most of them either run into the droplet region or to the most stable fixed point  $P_3$ , representing undershooting and overshooting saddle-point solutions where the latter behave as  $H(r) = (-\Delta\mu)r^2/[2(d-1)\sigma_{lv}]$

for  $r \rightarrow \infty$ . The basins of attraction for these two sets of trajectories are separated by a surface which is the support of the critical-hole trajectories.

For  $d < d_1$  the trajectories for critical holes at  $\Delta\mu < 0$  cannot to come close to the fixed point  $P_2$ . This is a consequence of the fact that, in agreement with (2.97), these trajectories for  $t \rightarrow \infty$  have to run to  $X = 0$ ,  $Y = Z = \infty$ . According to (2.105) they must, however, penetrate the plane  $X = 2/(m+1)$  above the line  $Z = (2/(m+1))(Y - Y_1)$ , and for  $X \geq 2/(m+1)$  obey the condition  $\dot{Y} \leq 0$ . This is incompatible with a visit of the fixed point  $P_2$  which consequently has no influence on the critical-hole profile for  $\Delta\mu < 0$ .

At bulk coexistence  $\Delta\mu = 0$  appears an infinite set of flow lines in the  $X, Y$ -plane running from  $X = Y = \infty$  to the fixed point  $P_2$ . As a consequence the saddle-point equation (2.95) for  $\Delta\mu = 0$  has infinitely many solutions which obey the boundary conditions for critical holes. Only one of these solutions will, however, correspond to a true minimum in the variational principle  $\delta\mathcal{H}/\delta h = 0$ .

The situation can most easily be analyzed in the special dimension  $d = d_0(m)$ . Here, in terms of the new variables

$$v(t) \equiv \left(\frac{r}{R_c}\right)^{-\frac{2}{m+1}} H(r), \quad t \equiv \ln\left(\frac{r}{R_c}\right), \quad (2.107)$$

the saddle-point equation (2.95) assumes the form

$$\ddot{v} = -\frac{\partial}{\partial v} \left[ \frac{A}{\sigma_{lv}} R_c^2 v^{1-m} + \frac{2}{(m+1)^2} v^2 \right] \quad (2.108)$$

which again can be considered as an equation of motion for a fictitious particle, but now without a friction term. As a consequence, the particle energy

$$\varepsilon \equiv \frac{1}{2} \dot{v}^2 - \frac{A}{\sigma_{lv}} R_c^2 v^{1-m} - \frac{2}{(m+1)^2} v^2 \quad (2.109)$$

is conserved. The last equation can be rewritten as

$$(x-1)^2 = \frac{2}{m-1} y - \lambda \frac{m+1}{m-1} y^{\frac{2}{m+1}} + 1 \quad (2.110)$$

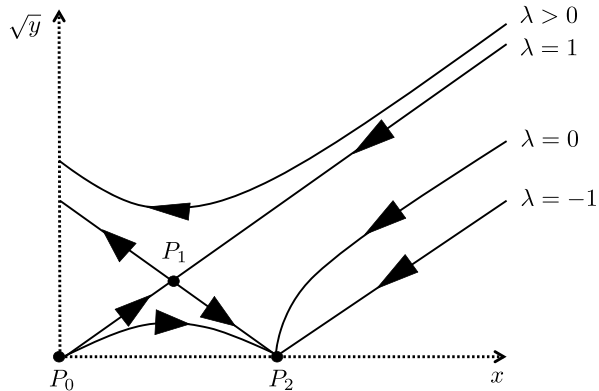
where

$$x \equiv \frac{X}{X_1}, \quad y \equiv \frac{Y}{Y_1}, \quad \lambda \equiv -\frac{\varepsilon}{\varepsilon_0}, \quad (2.111)$$

and  $\varepsilon_0 \equiv [2/(m^2-1)][(m-1)(m+1)^2 A R_c^2 / (4\sigma_{lv})]^{2/(m+1)}$  is the maximum value of the potential energy in (2.109). With  $\lambda$  taken as a parameter, Eq. (2.110) analytically describes the full flow pattern of the system which is depicted in Fig. 2.22.

Obviously this pattern is symmetric with respect to the line  $x = 1$ . For  $x = y = 1$  one obtains the parameter value  $\lambda = 1$  which consequently belongs to the separatrix running through the fixed point  $P_1$  (see Fig. 2.22). This corresponds to zero kinetic energy of the fictitious particle when it passes the maximum of the potential in (2.109). Values  $\lambda > 1$  accordingly belong to undershooting solutions, whereas for  $\lambda < 1$  one finds an infinite set of solutions obeying the critical-hole boundary

**Fig. 2.22** The flow pattern corresponding to Eq. (2.110) for the limiting case  $m = 3$ . (Note that  $H'(r = \infty) = 0$  for  $m = 3$ ) redrawn after Foltin et al. (1997)



conditions. The profile (2.101) leads to the value  $\lambda = 0$ , i.e., a simple parabola for the corresponding flow line.

For  $d = d_0(m)$  the energy functional  $\mathcal{H}[H(r)]$  can be written in the form

$$\mathcal{H} = \Omega_{d-1} [(m^2 - 1)AY_1^m / (2\sigma_{lv})]^{2/(m+1)} u[y] \quad (2.112)$$

where

$$u = \int_0^\infty dy \frac{y^{-\frac{m+3}{m+1}}}{2(x-1)} \left[ \frac{1}{2}x^2 + \frac{1}{m-1}y \right]. \quad (2.113)$$

This implies

$$\frac{\delta u}{\delta x(y)} = \frac{1}{4}y^{-\frac{m+3}{m+1}} \frac{1}{(x-1)^2} \left[ x^2 - 2x - \frac{2}{m-1}y \right], \quad (2.114)$$

which shows that the variational principle  $\delta u = 0$  leads to (2.110) with  $\lambda = 0$ . The special solution (2.101) therefore, in fact, corresponds to a true minimum of  $\mathcal{H}$ .

#### 2.5.4 Scaling Behaviour of the Critical Hole

We now turn to the characterization of the critical hole in terms of scaling quantities. These are the quantities  $H_c$ ,  $R_c$ , and  $E_c$  for a critical hole at arbitrary values of  $\Delta\mu$ . For this we use the definitions

$$\Phi'(H_c + h_0) = 0, \quad E_c \equiv \mathcal{H}[h(r)] - \mathcal{H}[H_c + h_0], \quad (2.115)$$

and extract  $R_c$  from the relation

$$\Phi(H_c + h_0) - \Phi(h_0) = (d-2)\sigma_{lv} \int_0^\infty dr r^{-1} (h'(r))^2, \quad (2.116)$$

implied by the saddle-point equation. The second Eq. (2.116) can slightly be simplified by use of the virial theorem which states that the potential-energy part in (2.115) is  $(3-d)/(d-1)$  times the kinetic part. This follows from the scaling property

$$\partial \mathcal{H}[h(\alpha r)] / \partial \alpha|_{\alpha=1} = 0 \quad (2.117)$$

which in turn is implied by the variational principle  $\delta\mathcal{H}[h_\alpha(r)] = 0$  for the special set of functions  $h_\alpha(r) \equiv h(\alpha r)$ . As a result we obtain

$$E_c = (d-1)^{-1} \Omega_{d-1} \sigma_{lv} \int_0^\infty dr r^{d-2} (h')^2 \quad (2.118)$$

where  $\Omega_{d-1}$  again is the volume of the  $(d-1)$ -dimensional unit sphere.

Close to the line  $\Delta\mu = 0$ ,  $S \leq 0$ , we can in (2.115)–(2.118) neglect the microscopic increment  $h_0$  to  $H_c$ , replace  $V(h)$  by its asymptotic form and insert for  $h(r)$  the macroscopic profile  $H(r)$ . This leads to the result

$$H_c = \frac{1}{(m-1)A} |\Delta\mu|^{-\frac{1}{m}} \quad (2.119)$$

for  $\Delta\mu \rightarrow 0$ , and, to leading order, to the equations

$$A H_c^{1-m} - \Delta\mu H_c - S = (d-2) \sigma_{lv} \int_{R_c+r_0}^\infty dr r^{-1} (H')^2(r), \quad (2.120)$$

$$E_c = \frac{\sigma_{lv} \Omega_{d-1}}{(d-1)} \int_{R_c+r_0}^\infty dr r^{d-2} (H')^2(r). \quad (2.121)$$

Here, a cut-off length  $r_0 \ll R_c$  has been introduced in order to remove the artificial singularity which, due to the extrapolation of  $V(h)$  down to small  $h$ , occurs at  $r = R_c$  in the case  $m \geq 3$ . In (2.120) and (2.121) we now split off integrals running from  $R_c + r_0$  to  $(1+\lambda)R_c$  where the choice  $0 < \lambda \ll 1$  allows to use Eq. (2.94). In the remaining integrals we transform to the scaled variables  $r/R^*$  for  $\Delta\mu < 0$  and  $r/R_c$  for  $\Delta\mu = 0$ , suggested by the asymptotic forms of the hole profiles. This leads to a power in  $R^*$  and  $R_c$ , respectively, where the cofactors are assumed to be finite in the limit  $h \rightarrow 0$  and  $S \rightarrow 0$ .

On a path  $S = \text{const.}$  in the partial-dewetting regime the procedure just described leads for  $|\Delta\mu| \rightarrow 0$  to a constant value of  $R_c$ , and to

$$E_c \sim H_c^{\frac{m+1}{2}(d-d_0(m))} \quad (2.122)$$

with  $H_c$  given by (5.4). At  $S = 0$ , i.e. in the complete-dewetting regime, we find the behaviour

$$\begin{aligned} R_c &\sim H_c^{\frac{m+1}{2}} && \text{for } m < 3, \\ R_c &\sim H_c^2 \ln H_c && \text{for } m = 3, \\ R_c &\sim H_c^{m-1} && \text{for } m > 3 \end{aligned} \quad (2.123)$$

where again  $H_c$  has the form (5.4). Moreover, in this regime we obtain

$$\begin{aligned} E_c &\sim R_c^{d-d_0(m)} && \text{for } m < 3, \\ E_c &\sim R_c^{d-2} \ln R_c && \text{for } m = 3, \\ E_c &\sim R_c^{d-2} && \text{for } m > 3. \end{aligned} \quad (2.124)$$

For critical holes at  $\Delta\mu = 0$  the only nontrivial result is the behaviour

$$\begin{aligned} R_c &\sim |S|^{-\frac{m+1}{2(m-1)}} && \text{for } m < 3, \\ R_c &\sim |S|^{-1} \ln |S| && \text{for } m = 3, \\ R_c &\sim |S|^{-1} && \text{for } m > 3 \end{aligned} \quad (2.125)$$

for  $|S| \rightarrow 0$ .

In the pre-dewetting regime the asymptotic behaviour of the pancake critical holes will, with growing distance from  $T_w$ , increasingly depend on the microscopic details of the potential  $\phi(h)$ . We therefore have to go back to the relations (2.116) and (2.118), in which we then use the fact that  $h'(r)$  is sharply peaked at the value  $r = R_c$ . This leads for any path  $S = \text{const.}$  to a constant value of  $F_c$  at the prewetting line  $\Delta\mu = \Delta\mu_p(T)$ , and to the relations

$$R_c \sim (\Delta\mu_p(T) - \Delta\mu)^{-1}, \quad (2.126)$$

$$E_c \sim (\Delta\mu_p(T) - \Delta\mu)^{2-d} \quad (2.127)$$

which are identical to those for pancake droplets. When the wetting transition point is approached along the prewetting line,  $H_c$  diverges as in (2.119).

The crossover lines, separating the pre-dewetting and the partial-dewetting regime from the intervening complete-dewetting regime (see Fig. 2.16), are of the form  $|\Delta\mu| \sim |S|^{\frac{m}{m-1}}$ . This is implied by Eq. (2.120) through which the spreading coefficient  $S$  enters the calculation in the form  $S + \text{const.}|\Delta\mu|^{\frac{m-1}{m}}$ .

We have achieved a complete description of the (scaling) properties of critical holes. Of course, in case a complete knowledge of system parameters can be achieved, it is possible to explicitly calculate the excess free energy of the critical holes and the nucleation rate, Eq. (2.79).

*Task. Calculate the Gaussian fluctuation spectrum of a critical hole, i.e., the second variation of the interface Hamiltonian  $\mathcal{H}$  at the hole profile. What can be said qualitatively about the lowest-lying modes? See our discussion of the elastic properties of the contact line.*

### 2.5.5 Undercooling a Thick Film: A Physical Interpretation, and Some Theory

In this section we will discuss the undercooling of a thick film in somewhat more detail. The peculiarity of the undercooling of thick films has indeed been encountered experimentally in both classical liquids and in helium films, we will discuss these results in the following chapter. The interpretation of the experiments has, however, suffered from some conceptual confusions which make it useful to address this point specifically before going to a description of the experiments.

Figure 2.19 shows an undercooling path that is typically encountered experimentally. The system is initially prepared in a thick film state, controlled by its distance from the coexistence line,  $\Delta\mu \rightarrow -0$ , on the gas side of the wetting phase diagram. The film is then undercooled to a point below the prewetting line. Here, one encounters a ‘strange’ situation, since the critical hole is almost infinite in size and excess free energy for  $\Delta\mu = -0$ , and strictly infinite at  $\Delta\mu = 0$ . Thermal nucleation is therefore strongly suppressed.

In view of our previous discussion, there is *nothing* strange with this: the bulk coexistence line is a natural continuation of the prewetting line, except for the fact that one of phases now is infinitely thick (gas = thickness 0, liquid = thickness  $\infty$ ). All along each coexistence line, the critical nucleus has (by definition) an infinite size and excess free energy. In this picture, the decay of the thick films is thermodynamically disfavoured since the undercooling path leads close parallel to the coexistence line. The reason for the observed large stability of an undercooled film is thus nothing *but the asymmetric topology of the wetting phase diagram*.

Two alternative discussions exist in the literature, and we briefly address why they fail. Schick and Taborek (1992) related the long lifetime of undercooled films to the divergence of the line tension at wetting. It is, however, hard to see how the line tension at wetting can influence a process which never encounters the wetting point, and hence this divergence. The singularity that is encountered comes from a critical hole of almost infinite size. Put in another way: the physics of the problem is unrelated to the line tension, since the topology of the phase diagram does not depend on it. For both diverging and finite line tensions, the undercooling problem is the same.

A second discussion is by Herminghaus and Brochard (2006), who mix two things; the problem of the asymmetry of the interface configuration—a point we addressed in the discussion of the contact line—and the presence of gravity, both of which are claimed to make our discussion obsolete. However, for any finite value of  $\Delta\mu < 0$  the critical hole exists and has a finite (but very large) excess free energy. No critical hole of finite excess free energy exists on *any* of the coexistence lines. And, finally, gravity does not play a role in this at all: when films become gravity-controlled, there is no wetting phase transition anymore, see Blossey and Olgischleger (1999). Our whole discussion only makes sense if gravitational effects are not affecting the systems which are solely controlled by dispersion forces.

To round-up this pre-discussion of experiment vs theory, it should be noted that the role of thermal nucleation of a hole in the film and the enormous stability of undercooled wetting layers is strongly affected by the presence of borders—remember the discussion of the dewetting binary fluid mixture in the Introduction. When the system is prepared such that a border is present from which either a thin or a thick film can invade the surface, this process is generally much faster than the nucleation of holes (or, as in the complex dewetting scenario in the Introduction, both processes actually compete).

## 2.6 Dewetting for an Unstable Film: Spinodal Decomposition

After this very detailed discussion of the properties of a metastable thick film state we can now attack the second, and in fact, at first sight formally simpler case, that of an unstable thick film. In order to discuss this case we return to the interface Hamiltonian (2.2) taken at coexistence,  $\Delta\mu = 0$ , and at  $d = 3$ :

$$\mathcal{H}[h] = \int d^2x \left[ \frac{\sigma_{lv}}{2} (\nabla h)^2 + V(h) \right], \quad (2.128)$$

and calculate the variation  $\delta\mathcal{H}/\delta h(x) = 0$  for a one-dimensional configuration, assuming translational invariance in the transverse direction, which yields

$$-\sigma_{lv}h''(x) + V'(h) = 0. \quad (2.129)$$

We are now interested in a perturbation of a homogeneous film of thickness  $h_0$ , at sufficiently large  $h$  such that only the asymptotic form of  $V(h)$  matters. We then perturb this film via

$$h(x, t) = h_0 + \varepsilon \exp(ikx) \quad (2.130)$$

and then obtain

$$\begin{aligned} M(h_0) &\equiv -\sigma_{lv}h''(x) + V''(h_0)h(x) = (-\sigma_{lv}q^2 + V''(h_0))\exp(ikx) \\ &= \sigma_{lv}(q_s^2 - q^2)\exp(ikx). \end{aligned} \quad (2.131)$$

We can find a wavelength  $\lambda_s \equiv 2\pi/q_s$

$$\lambda_s = (2\pi) \sqrt{\frac{\sigma_{lv}}{-V''(h_0)}}, \quad (2.132)$$

such that  $M(h_0) > 0$  for  $\lambda > \lambda_s$  and  $M(h_0) < 0$  for  $\lambda < \lambda_s$ . The wavelength thus defines a change of stability for the perturbation. The wavelength  $\lambda_s$  depends on the curvature of the interface potential; if for the latter we have  $A < 0$  in the asymptotic form,  $\lambda_s$  will be meaningful, which is indeed the case for an unstable film.

The wavelength we calculated turns out to be essentially the wavelength of *spinodal dewetting*. (The prefactor is not correct since we so far neglected the dynamics of the film which respects mass conservation; the real wavelength thus turns out to be larger by a factor of  $\sqrt{2}$ .) For wavelengths larger than  $\lambda_s$ , perturbations of the film will grow, while perturbations of shorter wavelength will relax. For the case of a van der Waals interface potential,  $\lambda_s \sim h_0^2$ .

The spinodal dewetting scenario has been postulated several times in the literature; the first appears to be by Vrij (1966). In the context of wetting phenomena, the most cited reference is Brochard-Wyart and Daillant (1989).

*Task. The previous calculation shows that for each film height  $h_0$  there is a characteristic wavelength  $\lambda_s$  such that for  $\lambda > \lambda_s$  the film is unstable to fluctuations. This calculation, however, ignores flow and mass conservation in the film. Assuming a Poiseuille flow one has*

$$j = C \frac{d}{dx} \mathcal{H}[h(x)], \quad (2.133)$$

where  $C = h^3/3\eta$ , where  $\eta$  is viscosity. Calculate the correct spinodal dewetting wavelength if in addition mass conservation in the film is assumed.

In order to close this chapter, we finally address the question of the range of validity of the effective interface approach, at least from a theoretical perspective. For this, we briefly address a more microscopic approach, *density functional theory*.

## 2.7 Density Functional Theory

The effective interface approach has allowed us to venture beyond the macroscopic concept of Young's equation to include *microscopic effects* on a *mesoscopic scale*: up to several tens of nanometers. Getting down into the nanometer range, our approach will certainly be pushed to its limits, if not beyond. Can we extend our concepts into that range? For more microscopic aspects, the use of *density functional theory* is a possibility. A basic review article on the method is by Evans (1979).

The basis of this approach is the *grand canonical free energy functional* of the number density  $\varrho(\mathbf{r})$  of a one-component fluid (Bauer and Dietrich 1999)

$$\begin{aligned} \Omega[\varrho(\mathbf{r}); T, \mu] = & \int_{\Lambda} d^3r f_{HS}(\varrho(\mathbf{r}), T) + \int_{\Lambda} d^3r [V(\mathbf{r}) - \mu] \varrho(\mathbf{r}) \\ & + \frac{1}{2} \int_{\Lambda} d^3r \int_{\Lambda} d^3r' \varrho(\mathbf{r}) w(|\mathbf{r} - \mathbf{r}'|) \varrho(\mathbf{r}') \end{aligned} \quad (2.134)$$

where  $\Lambda$  is a finite fluid volume in the half space  $\Lambda_+$  with  $z > 0$ , with  $\Lambda \rightarrow \Lambda_+$  in the thermodynamic limit. The external potential  $V(\mathbf{r})$  describes the interaction of a fluid particle with the substrate via

$$V(\mathbf{r}) = V(z > 0) = - \sum_{i \geq 3} \frac{u_i}{z^{i''}}. \quad (2.135)$$

An exemplary case would be a *Lennard-Jones potential*

$$\phi_v = 4\varepsilon_v \left[ \left( \frac{\sigma_v}{r} \right)^{12} - \left( \frac{\sigma_v}{r} \right)^6 \right] \quad (2.136)$$

where  $\varepsilon_v$  is the interaction strength and  $\sigma_v$  characterizes molecular size. We take with  $v = w$  and assume a lateral average for the wall-fluid interaction  $V$ , and with  $v = f$  for the attractive part of the pair potential between the fluid particles. Approximately, one has for  $w$  the expression

$$w(r) = \int d^3r w(r) = \frac{4w_0\sigma_f^3}{\pi^2} \frac{1}{(r^2 + \sigma_f^2)^3} \quad (2.137)$$

where  $w_0 \sim \varepsilon_f \sigma_f^3$ . The repulsive part of the interaction is modeled by the first term in Eq. (2.134) which is a reference free energy of a hard-sphere fluid in a *Carnahan-Starling approximation*

$$f_{HS}(\varrho, T) = k_B T \varrho \left( \ln(\varrho \lambda^3) - 1 + \frac{4\eta_p - 3\eta_p^2}{(1 - \eta_p)^2} \right) \quad (2.138)$$

where  $\lambda$  is the thermal de Broglie wavelength  $\lambda$ ,  $\eta_p = (\pi/6)\varrho d^3(T)$  the dimensionless packing fraction, and  $d(T)$  an effective hard-sphere diameter.

From this theory the bulk properties are easily derived by minimizing  $\Omega$  with respect to density, ignoring the wall-fluid interaction. The analysis of film properties then proceeds by introducing a ‘*sharp-kink approximation*’ in the form

$$\widehat{\varrho}(x, z) = \Theta(z - d_w) \{ \varrho_l \Theta(h(x) - z) + \varrho_g \Theta(z - h(x)) \} \quad (2.139)$$

where  $d_w$  is the location of the wall, and where  $h(x)$  asymptotically for large arguments approaches

$$\widehat{h}(x) = h_0 \Theta(-x) + (h_0 + x \tan \theta) \Theta(x), \quad (2.140)$$

with the contact angle  $\theta$ ; this corresponds to the situation we discussed already for the line tension.

From here on one can separate the contributions to the grand canonical free energy into bulk, surface and line contributions; we refer to Bauer and Dietrich (1999) and the references listed there for details. For our present purposes we state only the Euler-Lagrange equation for the film which is a *nonlocal* expression, due to the presence of the double integral over fluid space:

$$-\Delta\varrho \int_{-\infty}^{\infty} dx' \int_0^{h(x')-h(x)} dz' \overline{w}(|x-x'|, |z'|) = [V(h(x)) - \varrho_l t(h(x) - d_w)] \quad (2.141)$$

wherein  $w(x, z)$  and  $t(z)$  are defined as

$$\overline{w}(x, z) = \int_{-\infty}^{\infty} dy w(|\mathbf{r}|) \quad (2.142)$$

and

$$t(z) = \int_z^{\infty} dz' \int_{R^2} dx dy w(|\mathbf{r}|), \quad (2.143)$$

and  $\varrho_l$  is the liquid density,  $\Delta\varrho$  the density difference between the two bulk fluid phases (liquid/gas).

*How does this nonlocal theory deviate from the local theory we have used?* In fact, they differ not by much in the context of the sharp-kink description which underlies both the local theory and the present DFT treatment (Bauer and Dietrich 1999). Against earlier claims based on errors in the numerical treatment of Eq. (2.141), the nonlocal theory reproduces the results of the local theory for the line tension. The only noticeable differences arise with respect to interfacial curvatures. These findings therefore vindicate our treatment—in the limit of the desired precision.

However, there are real corrections to the capillary dispersion theory that can indeed be captured by a careful treatment of effects starting from the DFT. One can derive an effective interface Hamiltonian which correctly treats long-ranged effects, and then leads to a *wavevector-dependent surface tension*. We refrain from writing down the expression and refer the interested reader to the original derivation (Mecke and Dietrich 1999). Although this is indeed a subtle effect, it has been observed experimentally in water Fradin et al. (2000).

Thin Liquid Films

Dewetting and Polymer Flow

Blossey, R.

2012, XVIII, 154 p., Hardcover

ISBN: 978-94-007-4454-7